© 2019. Published by The Company of Biologists Ltd | Journal of Cell Science (2019) 132, jcs229179. doi:10.1242/jcs.229179

RESEARCH ARTICLE

SH3YL1 cooperates with ESCRT-I in the sorting and degradation of the EGF receptor

Junya Hasegawa[1,*], Imen Jebri[1,2], Hikaru Yamamoto[2,‡], Kazuya Tsujita[1,2], Emi Tokuda[3,*], Hideki Shibata[4], Masatoshi Maki[4] and Toshiki Itoh[1,2,§]

ABSTRACT

Ubiquitinated membrane proteins such as epidermal growth factor receptor (EGFR) are delivered to early endosomes and then sorted to lysosomes via multivesicular bodies (MVBs) for degradation. The regulatory mechanism underlying formation of intralumenal vesicles en route to generation of MVBs is not fully understood. In this study, we found that SH3YL1, a phosphoinositide-binding protein, had a vesicular localization pattern overlapping with internalized EGF in endosomes in the degradative pathway. Deficiency of SH3YL1 prevents EGF trafficking from early to late endosomes and inhibits degradation of EGFR. Moreover, we show that SH3YL1 mediates EGFR sorting into MVBs in a manner dependent on its C-terminal SH3 domain, which is necessary for the interaction with an ESCRT-I component, Vps37B. Taken together, our observations reveal an indispensable role of SH3YL1 in MVB sorting and EGFR degradation mediated by ESCRT complexes.

KEY WORDS: SH3YL1, Endosome, EGF, ESCRT, MVB

INTRODUCTION

Membrane proteins and lipids located at the cell surface, as well as extracellular fluids, are internalized into the cytosol through a variety of endocytic pathways (Doherty and McMahon, 2009; Mayor and Pagano, 2007; McMahon and Boucrot, 2011). It has been established that internalized molecules are delivered mainly via three alternative routes after reaching early endosomes. A group of membrane proteins including the transferrin receptor are recycled back to the plasma membrane, whereas others such as mannose 6-phosphate receptors and some bacterial toxins enter the *trans*-Golgi network. In the third route, membrane proteins such as epidermal growth factor receptor (EGFR) are sorted to late endosomes and lysosomes for degradation (Bonangelino et al., 2002; Grant and Donaldson, 2009; Maxfield and McGraw, 2004).

[1]Division of Membrane Biology, Department of Biochemistry and Molecular Biology, Kobe University Graduate School of Medicine, 7-5-1 Kusunoki-cho, Chuo-ku, Kobe, Hyogo 650-0017, Japan. [2]Biosignal Research Center, Kobe University, 1-1 Rokkodai-cho, Nada-ku, Kobe, Hyogo 657-8501, Japan. [3]Integrated Center for Mass Spectrometry, Kobe University Graduate School of Medicine, 7-5-1 Kusunoki-cho, Chuo-ku, Kobe, Hyogo 650-0017, Japan. [4]Department of Applied Biosciences, Graduate School of Bioagricultural Sciences, Nagoya University, Furo-cho, Chikusa-ku, Nagoya 464-8601, Japan.
*Present address: Department of Biochemical Pathophysiology, Medical Research Institute, Tokyo Medical and Dental University, 1-5-45, Yushima, Bunkyo-ku, Tokyo 113-8510, Japan. ‡Present address: Department of Neurophysiology and Neural Repair, Gunma University Graduate School of Medicine, Maebashi, Gunma 371-8511, Japan

§Author for correspondence (titoh@people.kobe-u.ac.jp)

T.I., 0000-0001-6433-1894

Received 20 December 2018; Accepted 29 August 2019

In the degradative endocytic pathway, ubiquitinated EGFR is loaded onto intraluminal vesicles (ILVs) inside late endosomes. This process involves hepatocyte growth factor-regulated tyrosine kinase substrate (Hrs) and endosomal sorting complex required for transport (ESCRT) complexes (Hurley and Hanson, 2010; Katzmann et al., 2001; Raiborg and Stenmark, 2009; Williams and Urbé, 2007). The current model proposes that the ubiquitin-binding Hrs and signal transducing adaptor molecule (STAM) protein complex bind to the endosomal lipid phosphatidylinositol 3-phosphate [PI(3)P] through the FYVE domain of Hrs (Raiborg et al., 2001). In early endosomes, the Hrs–STAM protein complex initiates the process of EGFR sorting to lysosomes (Raiborg et al., 2003; Slagsvold et al., 2006) by accumulating ubiquitinated EGFR to a specialized clathrin-coated area on endosomal membranes (Raiborg et al., 2002, 2006; Sachse et al., 2002). Subsequently, the EGFR sequentially interacts with the ESCRT-I, ESCRT-II and ESCRT-III complexes, which function in the invagination and formation of intraluminal membranes inside the endosome (Campsteijn et al., 2016; Im and Hurley, 2008; Olmos and Carlton, 2016; Raiborg et al., 2003). The inwardly invaginated membranes are finally subjected to a fission event to complete formation of the ILVs. Late endosomes containing the ILVs, referred to as multivesicular bodies (MVBs), then fuse with lysosomes for degradation (Hurley and Hanson, 2010; Slagsvold et al., 2006).

SH3 domain-containing Ysc84-like 1 (SH3YL1) protein has a unique lipid-binding domain, SYLF (named after the SH3YL1, Ysc84p (also known as Lsb4p), Lsb3p and plant FYVE proteins that contain it), which strongly binds to D5-phosphorylated phosphoinositides, such as phosphatidylinositol 3,4,5-trisphosphate [$PI(3,4,5)P_3$] (Hasegawa et al., 2011). Moreover, we have previously demonstrated that SH3YL1 is required for the formation of membrane ruffles at the dorsal side of the plasma membrane in response to growth factor stimulation (Hasegawa et al., 2011). Interestingly, it has been reported that the yeast homologs of SH3YL1, Lsb3p and Ysc84, are localized at intracellular vesicles together with an endocytic protein, Sla1p, and play an indispensable role in endocytosis (Dewar et al., 2002; Tonikian et al., 2009).

In this study, we elucidate the role of SH3YL1 in endosomal sorting of EGF. In HeLa cells, mCherry-tagged SH3YL1 displays a punctate localization pattern, which overlaps with that of CD63, a marker of late endosomes/MVBs. We show that in the absence of SH3YL1, EGF is not delivered to late endosomes even though it successfully proceeds through early endosomes. Furthermore, SH3YL1 directly interacts with an ESCRT-I component, vacuolar protein sorting-associated protein 37B (Vps37B), for EGFR degradation.

RESULTS

SH3YL1 is localized at late endosomes

To observe the intracellular localization of SH3YL1, HeLa cell lines that stably express mCherry-tagged SH3YL1 (SH3YL1–mCherry)

Journal of Cell Science (2019) 132, jcs229179. doi:10.1242/jcs.229179

were established and examined under a confocal microscope. Interestingly, SH3YL1–mCherry showed a vesicular localization in the cytosol (Fig. 1A, left panels). To confirm the identity of these SH3YL1–mCherry-positive vesicles, we co-stained the cells with antibodies against EEA1 and CD63, which are early and late endosome markers, respectively. As a result, it was revealed that the SH3YL1–mCherry-positive vesicles scarcely co-localized with EEA1-positive early endosomes (Fig. 1A, upper panels), whereas they abundantly overlapped with CD63-positive late endosomes (Fig. 1A, lower panels). In contrast, SH3YL1–mCherry did not overlap with transferrin receptor, a recycling endosome marker (Fig. S1A). These results indicate that SH3YL1 is closely associated with the degradative pathway but not with the recycling pathway.

Next, we examined whether SH3YL1 was involved in degradative endocytosis, using a pulse-chase assay that enabled us to monitor the transport of fluorescently labeled EGF internalized into the cell (see Materials and Methods). The EGF co-localized with SH3YL1–mCherry-positive vesicles after 5 min of internalization and a subsequent chase of 30 min (Fig. 1B, lower panels). However, this co-localization pattern was less pronounced after the first 10 min of the chase (Fig. 1B, upper panels), indicating that SH3YL1 plays a role in relatively mature endosomes on the EGF sorting route. Additionally, SH3YL1–mCherry-positive vesicles significantly co-localized with EGF receptor (EGFR) 30 min after EGF stimulation (Fig. S1B), confirming the involvement of SH3YL1 in the endocytosis of EGF–EGFR complex. These results collectively indicate that SH3YL1 is localized at late endosomes.

Depletion of SH3YL1 alters the distribution of endosomes in the degradative pathway

Knockdown experiments were carried out to study the function of SH3YL1 in endocytosis. We designed two different SH3YL1-targeted siRNAs and tested their ability to downregulate SH3YL1 protein levels in HeLa cells. The siRNA #2 was designed against the 3′ untranslated region (UTR) of the human SH3YL1 gene for subsequent rescue experiments. The expression of SH3YL1 was significantly reduced in cells transfected with either of the two siRNAs, but not with a control siRNA (Fig. S2A). Interestingly,

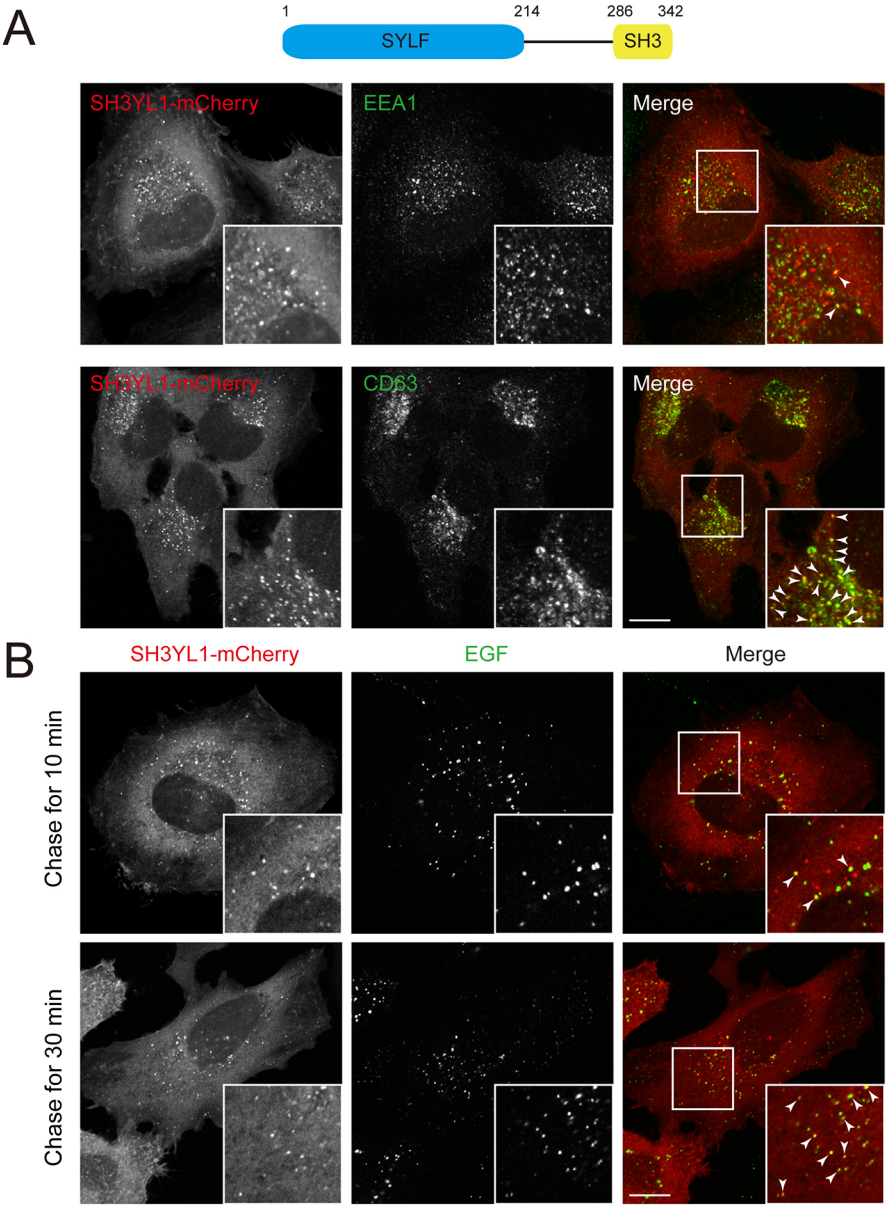

Fig. 1. SH3YL1 is localized at late endosomes. (A) Scheme of human SH3YL1 is given at the top. HeLa cells stably expressing SH3YL1–mCherry (red) are stained with anti-EEA1 (upper panels) or anti-CD63 (lower panels) antibodies (green). Arrowheads indicate co-localizations with Pearson correlation coefficients of 0.10±0.08 (SH3YL1–mCherry versus anti-EEA1) and 0.48±0.08 (SH3YL1–mCherry versus anti-CD63) (mean±s.d. of 10 cells). (B) HeLa cells stably expressing SH3YL1–mCherry (red) were incubated with 0.1 µg/ml Alexa Fluor 647-conjugated EGF (green) for 5 min at 37°C, and then chased in serum-free medium without markers for 10 min (upper panels) and 30 min (lower panels). Arrowheads indicate co-localizations. Images are representative of three independent experiments. Boxed regions are magnified in the insets. Scale bars: 10 µm.

Journal of Cell Science (2019) 132, jcs229179. doi:10.1242/jcs.229179

although the control siRNA-transfected HeLa cells had EEA1-positive early endosomes relatively close to the perinuclear region, a significantly dispersed localization pattern of early endosomes was observed in SH3YL1-depleted cells (Fig. 2A, upper panels). Localization of CD63-positive late endosomes, which were typically found at the perinuclear area of cells transfected with control siRNA, was also altered to a more dispersed pattern in SH3YL1-depleted cells (Fig. 2A, lower panels). The mean distance between the center of the nucleus and each endosomal vesicle, and the standard deviation, significantly increased, indicating that both early and late endosomes were more widely distributed throughout the cytosol of SH3YL1-depleted cells (Fig. 2B). These changes in the localization patterns were specific to degradative organelles, as the distributions of transferrin receptor and the Golgi marker GM130 were scarcely affected (Fig. S2B). In addition, knockdown of SH3YL1 had no effect on internalization and transport of transferrin to the perinuclear region (Fig. S2C). Given that intracellular transport of degradative endosomes toward the perinuclear region is highly correlated with their maturation from early to late endosomes (Jongsma et al., 2016; Korolchuk et al., 2011; Neefjes et al., 2017), the observed phenotype suggests that SH3YL1 has a key role in degradative endocytosis. Our findings suggest that SH3YL1 is involved in the cargo transport from early to late endosomes in the degradative pathway of endocytosis, but not in the recycling pathway.

Loss of SH3YL1 inhibits EGF trafficking to late endosomes

Next, we sought to determine whether SH3YL1 is essential for EGF transport through degradative endosomes. At early time points (after internalization for 5 min and subsequent chase for 0 and 10 min), internalized EGF reached EEA1-positive early endosomes in both the control and SH3YL1 knocked-down cells (Fig. 3A,B). Subsequently (chase for 30 min), the co-localization of EGF with EEA1 was decreased both in control and SH3YL1 knocked-down cells to the same extent, indicating that SH3YL1 is dispensable for travel of EGF through early endosomes.

Having confirmed that EGF was normally transported through early endosomes in the absence of SH3YL1, we next evaluated the involvement of SH3YL1 in EGF trafficking to late endosomes. After 30 or 60 min of the chase, images showed that EGF was successfully transported to CD63-positive late endosomes in control cells (30–40% co-localization; Fig. 4A,B). However, it was scarcely delivered to late endosomes in SH3YL1 knocked down cells, even after 60 min of the chase (~10% co-localization; Fig. 4A,B). These results suggest that SH3YL1 is necessary for EGF trafficking from early endosomes to late endosomes and/or MVBs.

Loss of SH3YL1 inhibits degradation of EGF receptor

To examine further the role of SH3YL1 in EGF trafficking, we performed the EGFR degradation assay in HeLa cells. In control cells, the protein levels of EGFR were strongly reduced at 40–60 min after EGF stimulation (Fig. 5A,B), indicating efficient degradation in lysosomes. In contrast, most of the EGFR remained intact even 60 min after EGF stimulation in SH3YL1 knocked-down cells (Fig. 5A,B).

Immunofluorescent staining of both control and SH3YL1 knocked-down cells showed that EGFR was internalized at 5 min after EGF stimulation with comparable levels (Fig. S3). In control cells, internalized EGFR was accumulated at the perinuclear region 30 min after EGF stimulation, but disappeared at 120 min, indicating effective degradation of EGFR (Fig. 5C, upper panels). In contrast, the distribution of internalized EGFR was more dispersed at 30 min in SH3YL1 knocked down cells and, more importantly, EGFR was detectable in the cells even 120 min after EGF stimulation (Fig. 5C, middle and lower panels). Based on these results, we conducted a rescue experiment using green fluorescent protein (GFP)-tagged SH3YL1 (SH3YL1–GFP) that encoded only the open reading frame of SH3YL1 and was therefore not targeted by siRNA#2 designed for the 3′-UTR. As a result, EGFR degradation was effectively recovered by the expression of SH3YL1–GFP (Fig. 6A,B). Interestingly, this rescue ability of exogenous SH3YL1 was lost when the SH3 domain was deleted (Fig. 6A,B). These results demonstrate that SH3YL1 is required for degradation as well as sorting of EGFR, and that these events depend on the C-terminal SH3 domain of SH3YL1.

SH3 domain of SH3YL1 is required for the formation of intraluminal vesicles

It has been reported that EGFR is transported through a subpopulation of MVBs to lysosomes for degradation (White et al., 2006), so we next examined whether SH3YL1 plays a role in formation of the ILVs that mediate EGFR sorting into MVBs. For this purpose, we utilized the ability of the active Rab5 mutant [Rab5(Q79 L)] to form enlarged

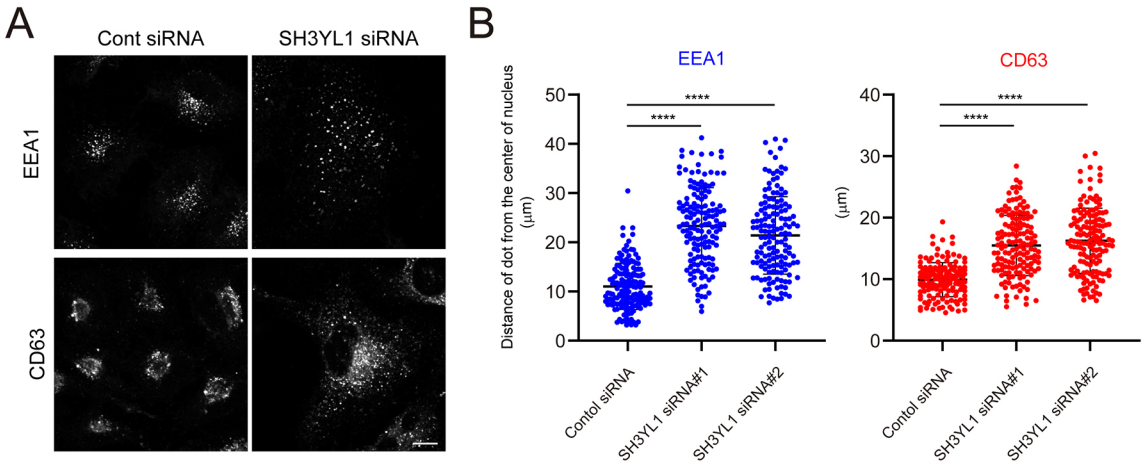

Fig. 2. Depletion of SH3YL1 alters the distribution of early and late endosomes. (A) HeLa cells treated with siRNAs (control or SH3YL1#2) were stained with anti-EEA1 or anti-CD63 antibodies. Images are representative of three independent experiments. (B) Distances (mean±s.d.) between the center of nuclei and each endosome (N=150, more than 10 cells) were measured using ImageJ software and are presented as scatter plots. ****P<0.0001 (Games–Howell multiple comparison test). Standard deviation values were significantly different, with P<0.0001 (Bartlett's test). Scale bar: 10 µm.

Journal of Cell Science (2019) 132, jcs229179. doi:10.1242/jcs.229179

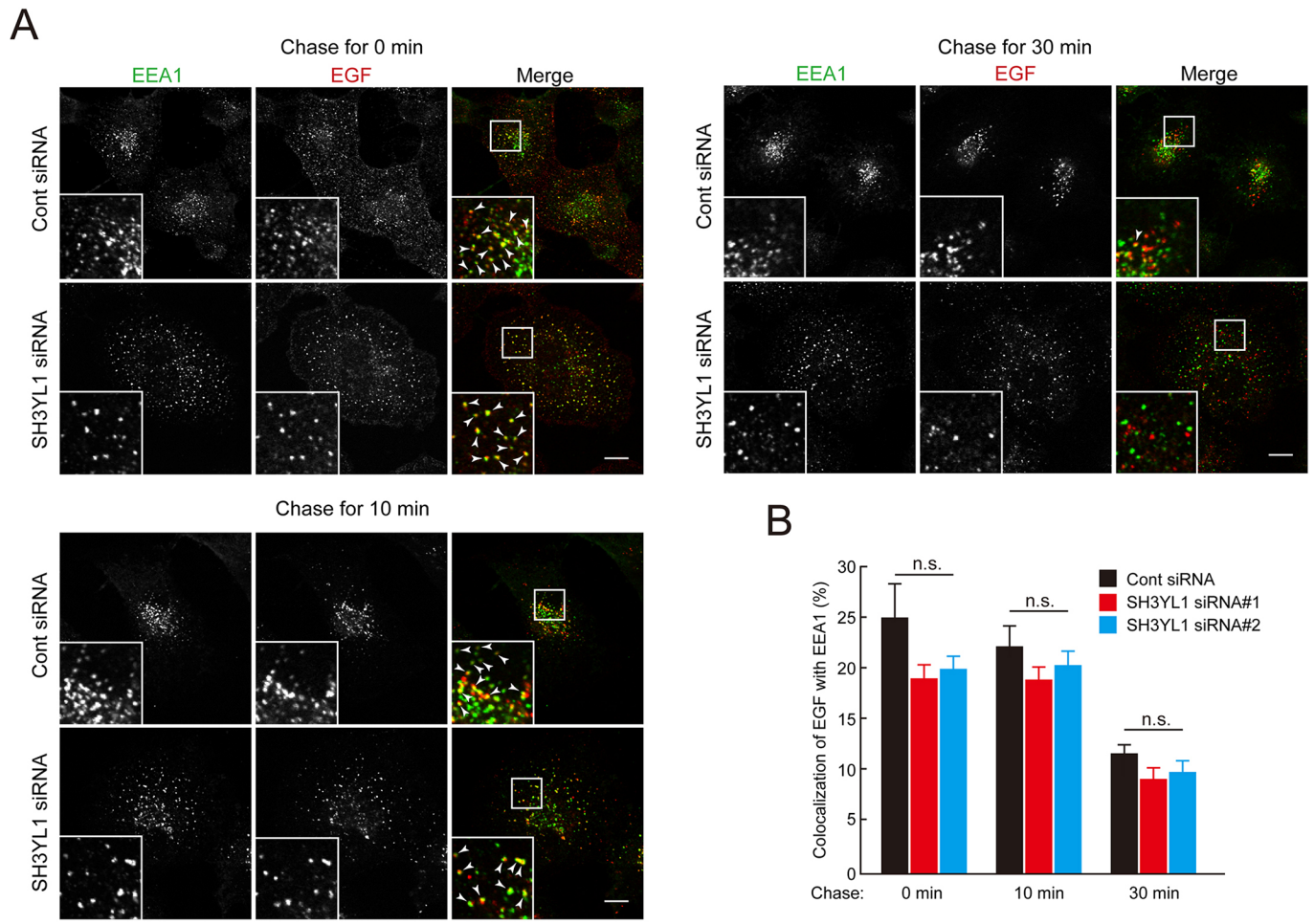

Fig. 3. Loss of SH3YL1 does not affect EGF trafficking via early endosomes. (A) HeLa cells treated with siRNAs (control or SH3YL1#2) were incubated with 0.1 µg/ml rhodamine–EGF for 5 min at 37°C and then chased in serum-free medium without EGF for 0, 10 and 30 min. Boxed regions are magnified in the insets. Arrowheads indicate co-localization of rhodamine–EGF (red) with EEA1 (green). Images are representative of three independent experiments. (B) Pixel-by-pixel co-localization analysis by Fluoview software was used to assess levels of rhodamine–EGF with EEA1. Ten random areas (as shown by the boxed areas) were picked up and measured. Results represent the mean±s.e.m. of 10 areas. n.s., not significant (Tukey's multiple comparison test). Scale bars: 10 µm.

early endosomes that provide high spatial resolution in confocal microscopy (Hanafusa et al., 2011; Pons et al., 2008, 2012; Raiborg et al., 2002; Trajkovic et al., 2008). At 15 min of EGF stimulation, cells treated with control siRNA displayed efficient translocation of EGFR to the ILVs inside the Rab5(Q79L)-induced enlarged endosomes (Fig. 7A). Quantification of immunostained EGFR showed that approximately 70% of the endocytosed EGFR was accumulated in the endosomal lumen (Fig. 7C). In contrast, both of the SH3YL1-targeting siRNAs used in this study significantly suppressed EGFR sorting into the lumen of the enlarged endosomes (Fig. 7A,C).

Furthermore, we performed rescue experiments to verify which region of SH3YL1 is essential for the incorporation of EGFR into the enlarged endosomes. Accordingly, expression of wild-type (WT) SH3YL1 or a lipid-binding defective mutant (M1) (Hasegawa et al., 2011) in the knockdown cells restored the appearance of EGFR in the lumen of enlarged endosomes (Fig. 7B,C). This observation suggests that the lipid-binding activity of SH3YL1 is not required for the formation of ILVs. However, expression of SH3YL1 (ΔSH3) or SH3YL1 (SYLF), both of which lack the C-terminal SH3 domain required for the protein–protein interaction, did not rescue the phenotype (Fig. 7B,C). These data reveal that the SH3 domain of SH3YL1 is necessary for transport of EGFR into the lumen of late endosomes.

SH3YL1 binds to an ESCRT-I component, Vps37B, for EGFR degradation

Based on the findings that the SH3 domain of SH3YL1 plays an important role in the sorting of EGFR to the ILVs in late endosomes, we searched the UniProt database (https://www.uniprot.org/) for any relevant interacting partners of SH3YL1 in this process. Interestingly, Vps37B, a component of the ESCRT-I subcomplex in mammals, is deposited as a significant binding protein of SH3YL1. The interaction between SH3YL1 and Vps37B has also been detected by a global two-hybrid screening (Yu et al., 2011). As the ESCRT-I subcomplex of the ESCRT machinery is known to recognize ubiquitinated cargo molecules such as EGFR and further induce membrane curvature for ILV formation, we decided to focus on this interaction.

First, GFP–Vps37B and FLAG–SH3YL1 (full length or ΔSH3 mutant) were co-expressed in 293FT cells and then the cell lysates were subjected to immunoprecipitation using anti-DYKDDDDK (FLAG) antibody. As shown in Fig. 8A, GFP–Vps37B co-precipitated with FLAG–SH3YL1 in a manner dependent on the SH3 domain of SH3YL1. The specificity of this interaction was investigated by an overlay assay using a recombinant SH3YL1 protein. It was found that, although weak binding to Vps37C was detected, SH3YL1 almost exclusively interacted with Vps37B out of the four human Vps37 proteins (Fig. S4A,B). The primary sequence

Journal of Cell Science (2019) 132, jcs229179. doi:10.1242/jcs.229179

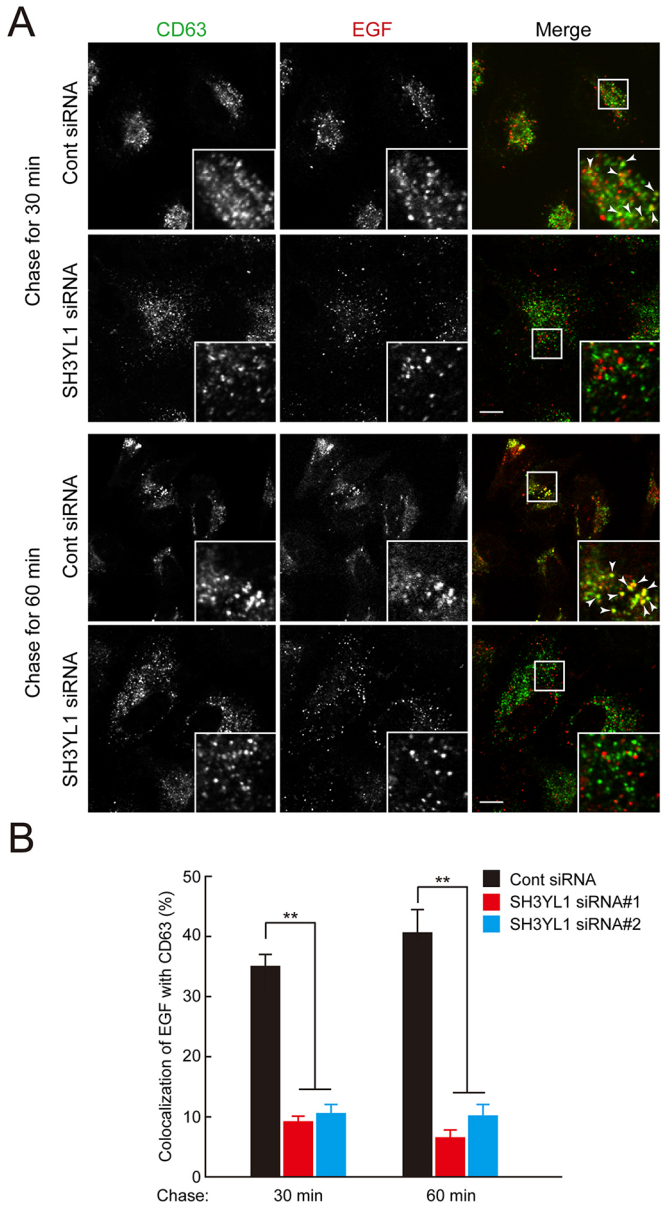

Fig. 4. SH3YL1 knockdown inhibits the transport of EGF to late endosomes. (A) HeLa cells treated with siRNAs (control or SH3YL1#2) were incubated with 0.1 µg/ml rhodamine–EGF for 5 min at 37°C and then chased in serum-free medium without EGF for 30 and 60 min. The boxed regions are magnified in the insets. Arrowheads indicate co-localization of rhodamine–EGF (red) with CD63 (green). Images are representative of three independent experiments. (B) Pixel-by-pixel co-localization analysis by Fluoview software was used to assess levels of rhodamine–EGF with CD63. Ten random areas (as shown by the boxed areas) were picked up and measured. Results represent the mean±s.e.m. of 10 areas. $^{**}P<0.01$ (Tukey's multiple comparison test). Scale bars: 10 µm.

of Vps37B has two PxLPxR consensus motifs (Fig. 8B) known to interact with the SH3 domain of mammalian SH3YL1 as well as their yeast homologs, Lsb3 and Lsb4 (Hasegawa et al., 2011; Tonikian et al., 2009). Indeed, SH3YL1 could not bind to Vps37B that lacked these motifs (Fig. 8C; Fig. S4C). Next, the localization of these two proteins was observed by confocal microscopy. In HeLa cells, stably expressed SH3YL1–mCherry co-localized with transfected GFP–Vps37B as well as EGF that was internalized for 20 min (Fig. 8D). Furthermore, knockdown of Vps37B resulted in significant delay of EGFR degradation, which was rescued by expression of wild-type Vps37B (1–285 amino acids), but not the Vps37B mutant that lacked PxLPxR motifs (1–173 amino acids) (Fig. 8E; Fig. S5). These data indicate that SH3YL1 binds to an ESCRT-I subcomplex component, Vps37B, and that this interaction is required for endosomal sorting and degradation of EGFR.

DISCUSSION

We demonstrate that SH3YL1 displays a punctate localization pattern that overlaps with that of CD63, a marker of late endosomes and MVBs, and that SH3YL1 is required for EGFR transport from early to late endosomes. In a previous study, we observed that transiently expressed SH3YL1 is localized to circular dorsal ruffles induced by platelet-derived growth factor, reflecting the ability of SH3YL1 to bind phosphoinositide at the plasma membrane (Hasegawa et al., 2011). We speculate that the different localization patterns between the previous and current studies are partly derived from the higher level of transient expressions in the previous study (Hasegawa et al., 2011). By establishing HeLa cell lines that stably express SH3YL1 with the C-terminal mCherry tag at lower levels, we observed vesicular localization patterns (Fig. 1). We also noticed that when co-expressed with its binding partner mediated by the SH3 domain (SHIP2, PI3KC2beta, Vps37B, etc.), SH3YL1 tends to be localized at vesicular structures (data not shown). This could be because of a possible 'open–close' conformational change that might be regulated by its C-terminal SH3 domain. Such a possibility is of great interest for future studies.

Our results indicate that SH3YL1 has an indispensable role in the sorting of EGFR to the ILVs in MVBs as well as in EGFR degradation. When SH3YL1 was knocked down in HeLa cells, both early and late endosomes changed their localizations from typical perinuclear positions to more dispersed patterns in the cytosol (Fig. 2A,B). There was also an apparent correlation between the distribution pattern of Rab5 (Q79L)-positive endosomes and the efficiency of EGFR sorting into the ILVs therein; enlarged endosomes with EGFR inside tended to accumulate more at the perinuclear region (Fig. 7A). Intracellular localization of degradative endosomes has been shown to correlate with their maturation status; early endosomes show a peripheral distribution pattern, whereas late endosomes tend to accumulate at the perinuclear 'clouds' (Jongsma et al., 2016; Korolchuk et al., 2011; Neefjes et al., 2017). Consistent with this, we showed that internalized EGF could not reach CD63-positive late endosomes in SH3YL1 knockdown cells (Fig. 4A,B). Thus, our results indicate the potential role of SH3YL1 in the maturation process of endosomes in the degradative pathway. As the internalized EGF could successfully travel through EEA1-positive early endosomes even in the absence of SH3YL1 (Fig. 3A,B), its site of action is likely to fall between early and late endosomes. As yet, the identity of endosomes that EGF–EGFR sorts into after SH3YL1 knockdown remains unclear. Our data show that internalized EGF could also travel through endosomes marked by GFP–Vps37B (Fig. S6). Therefore, the internalized EGF–EGFR in SH3YL1 knockdown cells might have been sorted to endosomes positive for ESCRT-II, ESCRT-III or other regulatory proteins such as the sorting nexin family (Cullen, 2008).

In this study, we confirmed a previous finding that a component of the ESCRT-I complex, Vps37B, is a binding partner of SH3YL1 (Yu et al., 2011). Vps37B is one of the four human Vps37 proteins, which associate with another ESCRT-I component, Tsg101, via their central stalk regions called the mod(r) domains (Bache et al., 2004; Boura et al., 2012; Okumura et al., 2013). Because of a helical bundle structure built by the stalk regions, ESCRT-I has an elongated shape

Journal of Cell Science (2019) 132, jcs229179. doi:10.1242/jcs.229179

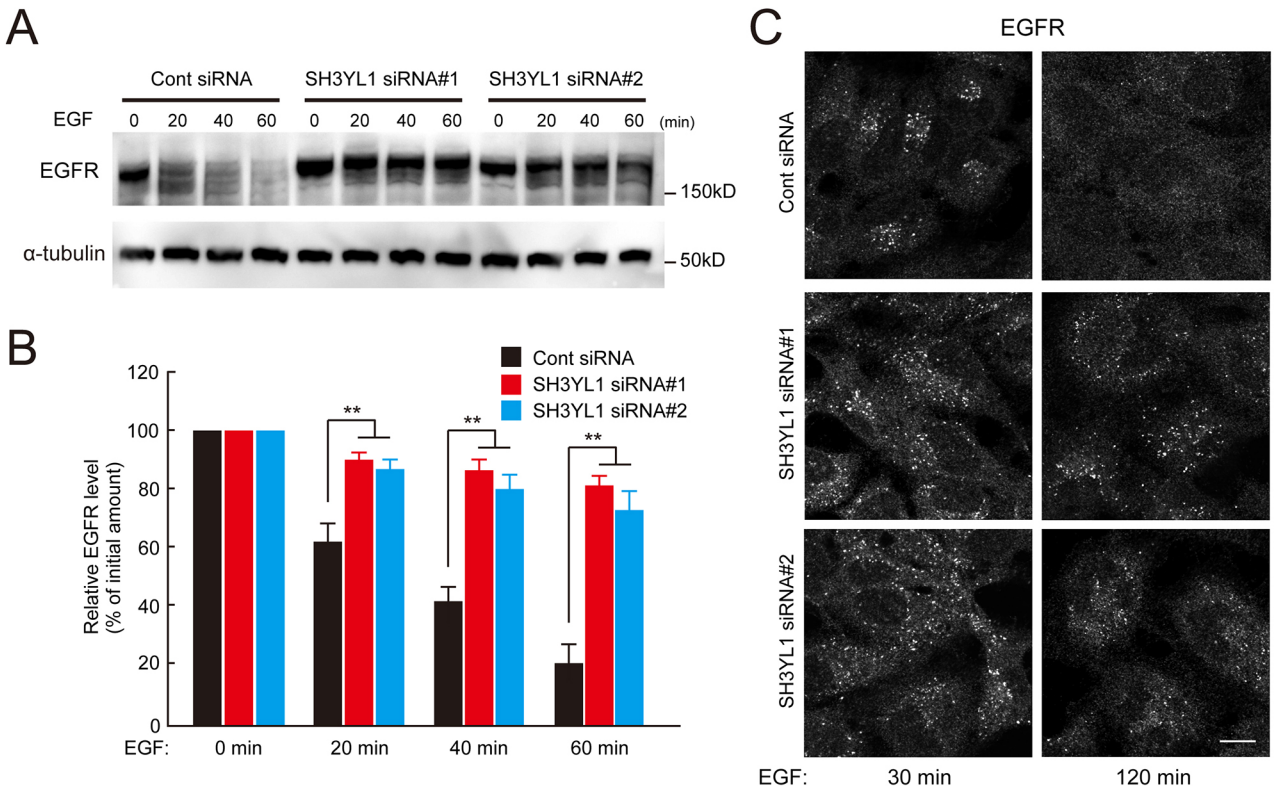

Fig. 5. Depletion of SH3YL1 suppresses EGFR degradation. (A) HeLa cells treated with siRNAs (control, SH3YL1#1 or SH3YL1#2) were stimulated with 50 ng/ml EGF for the indicated time periods. Cell lysates were analyzed by immunoblotting with anti-EGFR antibody. (B) Quantification of EGFR degradation shown in A, using ImageJ software. The results represent the mean±s.d. of three independent experiments. $^{**}P<0.01$ (Tukey's multiple comparison test). (C) HeLa cells were stimulated with 50 ng/ml EGF for 30 or 120 min, fixed and then immunostained with anti-EGFR antibody. Images are representative of three independent experiments. Scale bar: 10 µm.

that connects ESCRTs I and III (Boura et al., 2012; Henne et al., 2011; Hurley and Hanson, 2010; Kostelansky et al., 2006). Stenmark and colleagues identified the mammalian Vps37 genes and demonstrated that knocking down Vps37A significantly retarded the degradation of EGFR in lysosomes (Bache et al., 2004). In the current study, we show that Vps37B also plays a significant role in EGFR degradation in HeLa cells (Fig. 8E). It should also be noted that Vps37B knockdown resulted in a weaker effect on EGFR degradation than SH3YL1 knockdown (about eight times more EGFR-positive endosomes remained at 120 min in SH3YL1 knockdown cells compared with the control versus about three times more EGFR-positive endosomes in Vps37B knockdown cells compared with the control). We speculate that this may be because of a possible redundancy with other Vps37 proteins such as Vps37A or Vps37C. Vps37B has a proline-rich domain (PRD) at its C-terminal region, as do other Vps37 proteins such as Vps37C and Vps37D. We have previously demonstrated that the SH3 domain of SH3YL1 preferentially binds to a PxLPxR motif in the N-terminal PRD of SHIP2 (Hasegawa et al., 2011). Here, we demonstrate that Vps37B, but not Vps37C or Vps37D, has two PxLPxR motifs and that deletion of these motifs abrogated binding of Vps37B to SH3YL1 (Fig. 8C). In line with this result, co-localization with SH3YL1 was only observed for Vps37B, but not for Vps37C (data not shown).

Our data reveal that SH3YL1 plays an important role in the sorting of EGFR into the ILVs (Fig. 7) as well as its degradation therein (Figs 5,6). During the process of ILV formation, ESCRT-I is believed to trigger membrane invagination toward the lumen of late endosomes. Structural studies have collectively proposed a model in which the elongated and slightly curved shape of the ESCRT-I subcomplex is deployed on the surface of endosomal membrane, thereby inducing a negative membrane curvature for ILV formation (Boura et al., 2011, 2012). We have previously reported that SH3YL1 is involved in the formation of circular dorsal ruffles (CDRs) in response to PDGF stimulation (Hasegawa et al., 2011). It is noteworthy that the protrusive plasma membrane sculpted upon CDR formation retains a negative membrane curvature like that induced by the ESCRT complex. Based on the fact that SH3YL1 directly interacts with a component of ESCRT-I subcomplex, we speculate that SH3YL1 contributes to the membrane invagination process at the initial step of ILV formation. Indeed, our rescue experiments after SH3YL1 knockdown indicate that EGFR sorting into the ILVs and its subsequent degradation are dependent on the presence of the SH3 domain of SH3YL1, which directly binds to Vps37B (Figs 6,7).

It has been proposed that phosphoinositides, especially PI(3)P and PI(3,5)P_2, are the key molecules that regulate cargo trafficking from early to late endosomes (Hasegawa et al., 2017; McCartney et al., 2014). In fact, a variety of phosphoinositide-binding proteins, such as Hrs (Bache et al., 2003; Lu et al., 2003), Vps36 (Hierro et al., 2004; Im and Hurley, 2008), Vps22 (Teo et al., 2006), SNX3 (Pons et al., 2008) and SNX12 (Pons et al., 2012) have been reported to be involved in ILV biogenesis. Whereas most of these proteins preferentially bind to PI(3)P, the involvement of PI(3,5)P_2-specific binding partners in MVB formation is not fully understood. We have previously revealed that SH3YL1 binds strongly to D5-phosphorylated phosphoinositides, including PI(3,5)P_2, PI(4,5)P_2 and PI(3,4,5)P_3 (Hasegawa et al., 2011). However, our rescue experiments show that the M1 mutant of SH3YL1 [a PI(4,5)P_2- and PI(3,4,5)P_3-binding defective mutant] (Hasegawa et al., 2011) was

Journal of Cell Science (2019) 132, jcs229179. doi:10.1242/jcs.229179

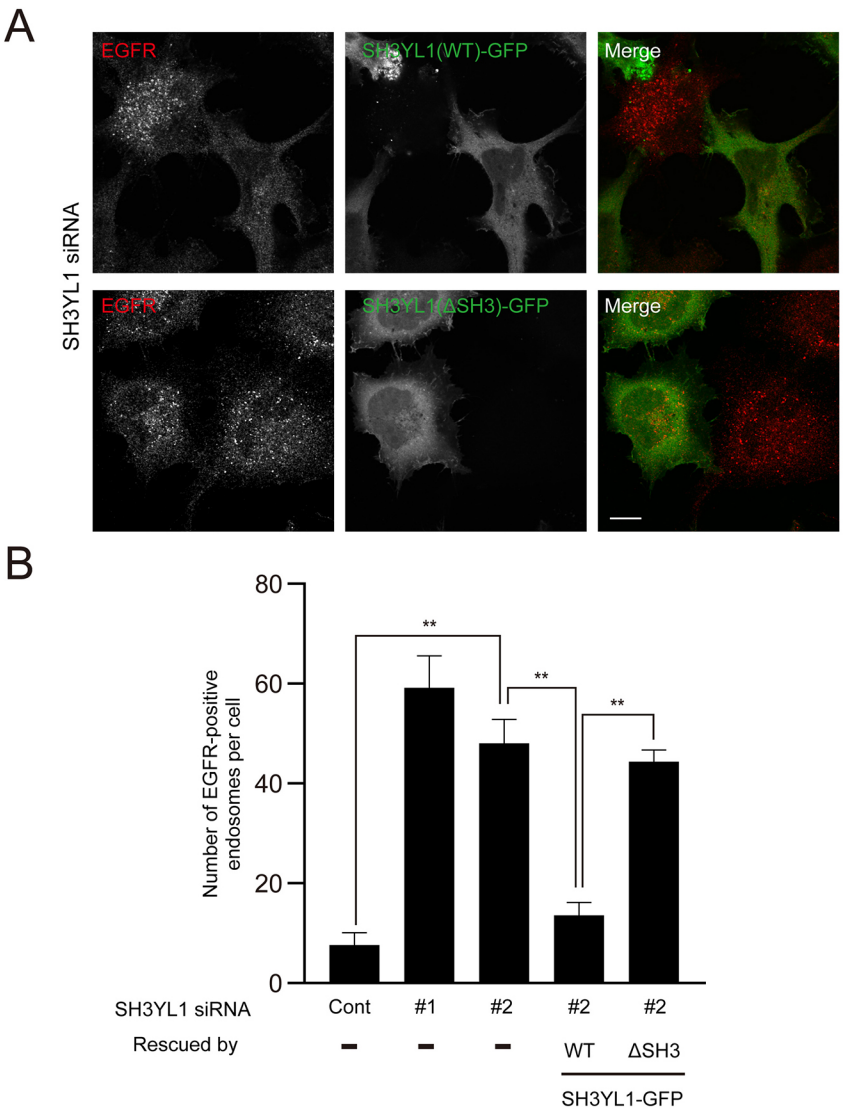

Fig. 6. The SH3 domain of SH3YL1 is required for EGFR degradation. (A) Rescue experiments by SH3YL1 constructs. HeLa cells treated with SH3YL1 siRNA#2 were transfected with SH3YL1(WT)–GFP or SH3YL1(ΔSH3)–GFP (green). After stimulation with 50 ng/ml EGF for 120 min, cells were immunostained with anti-EGFR antibody (red). Images are representative of three independent experiments. (B) EGFR-positive endosomes were counted and the results presented as the mean ±s.e.m. of three independent experiments with at least 20 cells per experiment. $^{**}P<0.01$ (Tukey's multiple comparison test). Scale bar: 10 µm.

able to recover the knockdown phenotype (Fig. 7C). This mutant also lacks affinity to PI(3,5)P_2 (Fig. S7A). In addition, the vesicular localization of SH3YL1–mCherry was not affected by treatment with apilimod, an inhibitor of PIKfyve which generates PI(3,5)P_2 (Fig. S7B) (Cai et al., 2013). Thus, further studies are needed in order to identify a PI(3,5)P_2-binding protein that regulates MVB formation and EGFR sorting into the ILVs.

MATERIALS AND METHODS

Reagents and antibodies

Rabbit anti-SH3YL1 polyclonal antibody was purchased from Sigma (HPA030926; 1:200). Mouse anti-EEA1 (clone 14; 1:100) and anti-GM130 (clone 35; 1:100) monoclonal antibodies were purchased from BD Biosciences. Mouse anti-α-tubulin monoclonal antibody (10G10; 1:2000) was from Wako. Rabbit anti-EGF receptor polyclonal antibody (Sc-03; 1:1000) and mouse anti-EGF receptor monoclonal antibody (A-10; 1:1000) were from Santa Cruz Biotechnology. Mouse anti-CD63 monoclonal antibody (clone RFAC4; 1:100) was from Millipore. Mouse anti-transferrin receptor monoclonal antibody (H68.4; 1:100) was from Zymed Laboratories. Mouse anti-DYKDDDDK (FLAG) monoclonal antibody (clone 1E6; 1:1000) was from Wako. Mouse anti-His monoclonal (OGHis; 1:1000) and rabbit anti-GFP polyclonal (598; 1:1000) antibodies were from MBL. All fluorescent reagents [tetramethylrhodamine-conjugated EGF, Alexa Fluor 647-conjugated EGF, Alexa Fluor 568-conjugated transferrin and Alexa Fluor 488-, 568-, 647-conjugated goat anti-rabbit or anti-mouse secondary antibodies (1:1000)] were purchased from Thermo Fisher Scientific. Recombinant human EGF was from R&D Systems (236-EG) and Wako (059-07873).

Plasmids

SH3YL1–GFP (wild type, M1, ΔSH3 and SYLF domain) and FLAG–SH3YL1 (wild type and ΔSH3) expression plasmids were constructed as described previously (Hasegawa et al., 2011). In brief, SH3YL1 cDNAs were ligated into the *Bgl*II and *Sal*I sites of pEGFP-N3 (Clontech) or the *Bam*HI and *Sal*I sites of pCMV-Tag2 (Agilent) mammalian expression vectors. Retroviral expression construct of SH3YL1–mCherry was made by PCR amplification of corresponding cDNA and subsequent ligation into the *Bam*HI and *Eco*RI sites of pQCXIP vector (Clontech). For bacterial expression, SH3YL1 cDNAs (wild type, M1 and M2) were ligated into the *Nde*I and *Xho*I sites of pET21 (Novagen) or the *Bam*HI and *Sal*I sites of pGEX 6P-1 (GE Healthcare) vectors. Human Rab5a (Q79L) cDNA was inserted into the *Bgl*II and *Bam*HI sites of pEGFP-C1 vector (Clontech). Human Vps37A, B, C and D cDNAs were ligated into the *Eco*RI and *Sal*I sites of pEGFP-C3 vector (Clontech) (Okumura et al., 2013).

Cell culture and transfection

HeLa, GP2-293 and 293FT cells were maintained in DMEM supplemented with 10% FBS. These cell lines were obtained from the American Type Culture Collection (ATCC) or purchased from Thermo Fisher Scientific and

Journal of Cell Science (2019) 132, jcs229179. doi:10.1242/jcs.229179

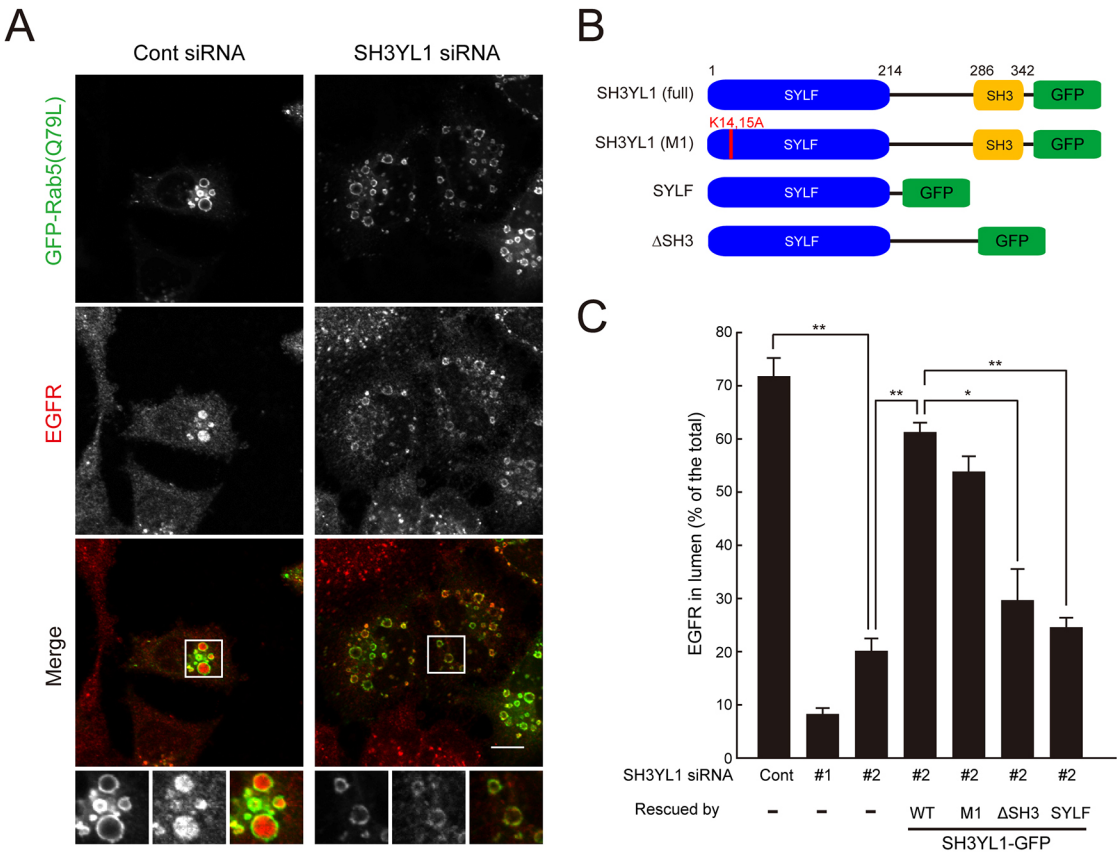

Fig. 7. SH3YL1 is indispensable for the formation of ILVs. (A) HeLa cells were treated with siRNAs (control or SH3YL1#2) and transfected with GFP–Rab5a(Q79L) (green) during the last 24 h. Subsequently, cells were incubated with 100 ng/ml EGF for 5 min at 37°C, chased in serum-free medium without EGF for 15 min and then stained with anti-EGFR antibody (red). Boxed regions are magnified in the insets. Images are representative of three independent experiments. (B) SH3YL1 constructs used for rescue experiments. M1 mutant has amino acid substitutions of $Lys^{14}Lys^{15}$ to $Ala^{14}Ala^{15}$. (C) Rescue experiments were performed by transfecting the SH3YL1–GFP constructs shown in B together with RFP-Rab5a(Q79L). The relative amount of EGFR in the lumen of Rab5a(Q79L)-induced enlarged endosome was quantified. Results represent the mean±s.d. of three independent experiments with at least 50 endosomes per experiment. *P<0.05, **P<0.01 (Tukey's multiple comparison test). Scale bar: 10 µm.

were regularly tested for mycoplasma contamination. Plasmid transfection was performed using FuGENE HD (Promega) for microscopic evaluation or Polyethylenimine Max (Polysciences) for biochemical assays. Experiments were carried out 24 h after transfection.

Retroviral expression and stable cell lines

GP2-293 cells were simultaneously transfected with pVSV-G and pQCXIP-SH3YL1-mCherry constructs for 48 h. Retroviral particles were saved in the culture medium, passed through a 0.45 µm filter and then added to HeLa cells with 4 µg/ml of polybrene. Stable cell lines were selected by serial dilutions in the presence of 2 µg/ml puromycin.

Co-immunoprecipitation assay

293FT cells were transfected with expression plasmids and further cultured for 48 h. After rinsing with PBS twice, cells were lysed in lysis buffer (50 mM Tris-HCl pH 7.4, 150 mM NaCl, 5 mM EDTA, 1% NP-40), briefly sonicated and then pre-cleared by centrifugation at 100,000 ***g*** for 10 min. The cell lysate in the supernatant was further incubated with anti-DYKDDDDK (FLAG) antibody immobilized on SureBeads Protein G magnetic beads (Bio-Rad) for 1 h with continuous rotation at 4°C. Beads were washed five times with lysis buffer and then bound proteins were eluted in SDS sample buffer. Co-immunoprecipitation was evaluated by immunoblotting with anti-GFP.

Overlay assay

Each Vps37 protein was expressed in 293FT cells, immunoprecipitated with anti-GFP as above and transferred onto PVDF membrane. After blocking with 5% skim milk in 0.05% Tween-20 in PBS (PBST) for 1 h, the membrane was incubated for 1 h with 0.5 µg/ml of recombinant SH3YL1-His protein in PBST and then with anti-His monoclonal antibody for 1 h. SH3YL1 protein bound to Vps37 protein was detected using horseradish peroxidase-conjugated anti-mouse secondary antibody (115-035-146, Jackson ImmunoResearch; 1:5000) and chemiluminescence (Chemi-Lumi One L, Nacalai).

RNA interference

For knockdown experiments, stealth siRNAs (Life Technologies) or ON-TARGETplus siRNAs (Dharmacon) targeting the respective human transcripts were designed as follows: 5′-AACAGCUCCCUUCUAAAGA-CACGCC-3′ (SH3YL1 siRNA#1), 5′-GCUAAGCAUUUGAUCUGGC-CAUGUA-3′ (SH3YL1 siRNA#2), 5′-AGUUGUGUGUGCCGGGUUA-3′ (Vps37B siRNA#1) and 5′-TGGCACCTGTTGACGGAAA-3′ (Vps37B siRNA#2). SH3YL1 siRNA#2, Vps37B siRNA#1 and Vps37B siRNA#2 corresponded to sequences in 3′-UTR for rescue experiments. The siRNAs (20 nM) were transfected into HeLa cells with Lipofectamine RNAiMAX (Life Technologies) and expression levels assessed after 72 h by immunoblots for SH3YL1 or reverse transcription and polymerase chain reaction (RT-PCR) for Vps37B.

RT-PCR

Total RNA was extracted using TRIzol (Thermo Fisher Scientific) and then reverse-transcribed with PrimeScript RT Master Mix (Takara). Expression levels of human Vps37B and GAPDH were examined by PCR using the following primers: 5′-AGATGGAGGAGACACAGAATGT-3′(Vps37B forward), 5′-TGCTAACAGGGTCTCCAAGG-3′ (Vps37B,

Journal of Cell Science (2019) 132, jcs229179. doi:10.1242/jcs.229179

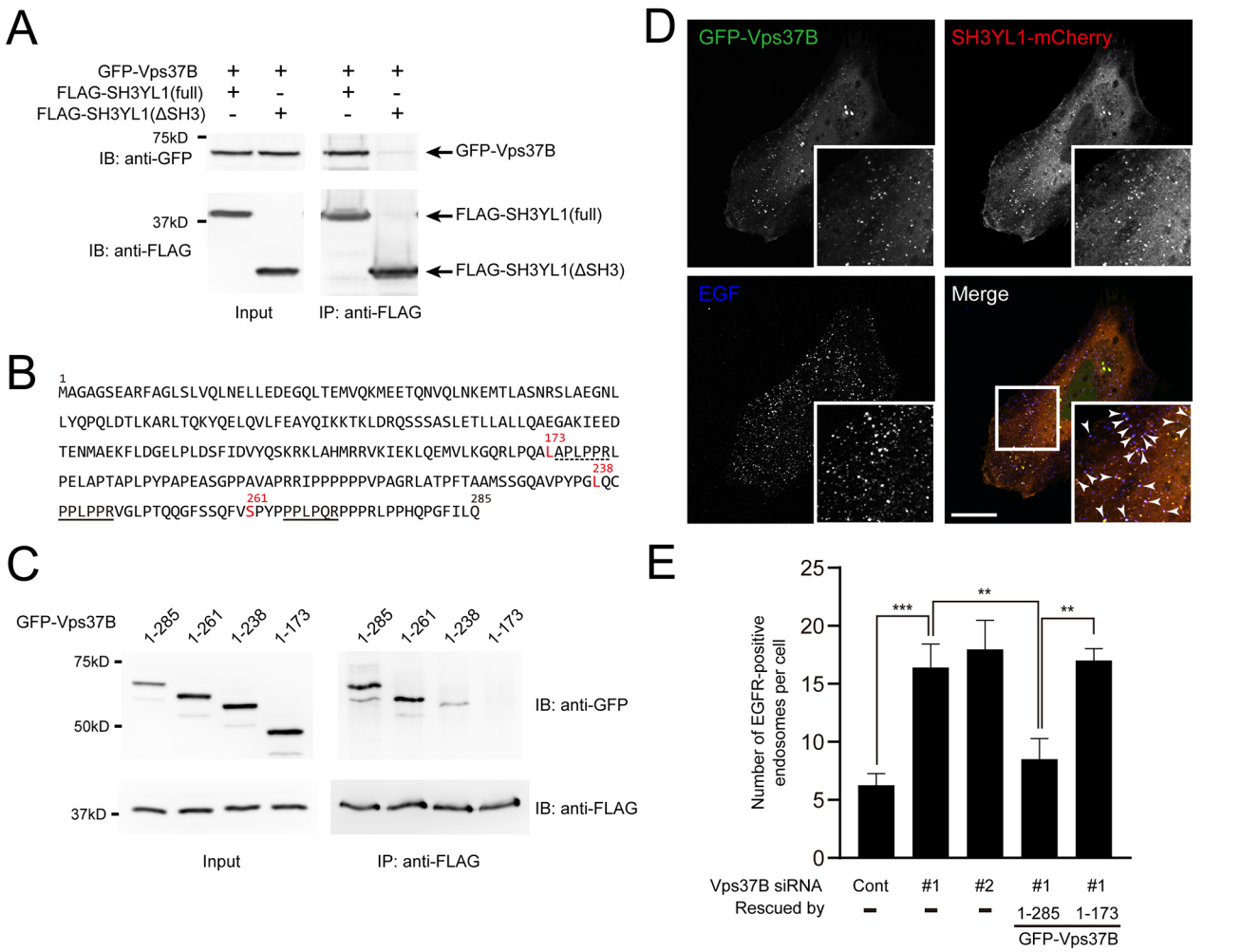

Fig. 8. SH3-dependent interaction between SH3YL1 and Vps37B is necessary for EGFR degradation. (A) The indicated constructs were simultaneously transfected into 293FT cells for 48 h and cell lysates prepared. SH3YL1 proteins were immunoprecipitated with anti-FLAG antibody and then analyzed by immunoblotting with anti-GFP antibody. Input: cell lysate. Data are representative of three independent experiments. (B) The amino acid sequence of human Vps37B. PxLPxR motifs are indicated by solid underline. An APLPPR sequence, which partially matches the PxLPxR consensus, is indicated by dashed underline. C-termini of deleted mutants are shown in red. (C) SH3YL1–Vps37B interaction requires PxLPxR motifs in Vps37B. The indicated constructs of GFP–Vps37B were analyzed by co-immunoprecipitation assay as in A. Data are representative of three independent experiments. (D) HeLa cells stably expressing SH3YL1–mCherry (red) were transfected with GFP–Vps37B (green) plasmids for 24 h. Transfected cells were incubated with 0.1 µg/ml Alexa Fluor 647–EGF (blue) for 5 min at 37°C and then chased in serum-free medium without EGF for 15 min before fixation. Boxed regions are magnified in the insets. Arrowheads indicate simultaneous co-localizations of three fluorescent signals. Images are representative of three independent experiments. (E) Knockdown of Vps37B in HeLa cells and rescue by wild-type (1–285) or PxLPxR motif-deleted mutant (1–173) of GFP–fGFPVps37B constructs. After stimulation with 50 ng/ml EGF for 120 min, cells were immunostained with anti-EGFR antibody. The numbers of EGFR-positive endosomes are shown as the mean±s.e.m. of three independent experiments with at least 20 cells per experiment. $^{**}P<0.01$, $^{***}P<0.001$ (Tukey's multiple comparison test). Scale bar: 10 µm.

reverse), 5′-GGAAGGTGAAGGTCGGAGTC-3′ (GAPDH, forward) and 5′-CTCGCTCCTGGAAGATGGTG-3′ (GAPDH, reverse).

Endocytosis assay

For EGF or transferrin uptake, cells were starved in serum-free medium for 1 h. Cells were first allowed to uptake fluorescently labeled markers by incubation with tetramethylrhodamine- or Alexa Fluor 647-conjugated EGF (0.1 µg/ml) or Alexa Fluor 568-conjugated transferrin (1 µg/ml) in DMEM for 5 min at 37°C. Subsequently, the medium was removed and the cells chased in a serum-free medium without fluorescent markers for the indicated time periods. For EGF receptor degradation, cells were starved in serum-free medium for 1 h and then incubated with 50 ng/ml EGF for the indicated time periods. Cell lysates were analyzed by immunoblots. Quantification of EGF receptor distribution in the lumen or on the limiting membrane of enlarged endosomes induced by Rab5 (Q79L) has been described (Trajkovic et al., 2008). To evaluate EGFR degradation by immunofluorescence, all images were obtained by confocal microscopy with a constant laser power and photomultiplier sensitivity. The obtained images were processed with ImageJ software to generate an automated threshold, and then EGFR-positive vesicles were counted.

Immunofluorescence microscopy

Cells were fixed with 3.7% formaldehyde in PBS for 10 min at room temperature (RT), permeabilized with PBS containing 0.2% Triton X-100 for 5 min at RT and then washed three times with PBS. Cells were incubated with primary antibodies in PBS for 90 min. After three washes with PBS, cells were incubated with the appropriate secondary antibodies in PBS for 1 h. After a brief wash with PBS, coverslips were mounted onto slides using PermaFluor Mountant Medium or ProLong Diamond Antifade Mountant (ThermoFisher Scientific) and observed under a FluoView 1000-D confocal microscope (IX81; Olympus) equipped with 473-, 568- and 633-nm diode lasers (Olympus) through an objective lens (60× oil immersion objective, NA 1.35; Olympus) and with Fluoview software (Olympus). Acquired images were processed with Photoshop (Adobe).

Co-localization and statistical analysis

A pixel-by-pixel co-localization analysis, using Fluoview (Olympus) or ImageJ software, was used to assess levels of co-localization between endosomal markers in confocal images. Statistically significant differences were determined using one-way ANOVA with Tukey's multiple comparisons test. Differences were considered significant if $P<0.05$.

Liposome co-sedimentation assay

Recombinant GST-fusion SH3YL1 (wild type, M1 and M2) proteins were expressed in BL21 bacterial strain and then purified with glutathione Sepharose 4B (GE Healthcare) according to the manufacturer's instruction. Removal of GST was performed by on-column cleavage using PreScission protease (GE Healthcare). Mixtures of PE (70%; Avanti Polar Lipids), PC (20%; Avanti Polar Lipids) and PI(3,5)P_2 (10%; CellSignals) were dried under nitrogen gas and suspended in 50 µl of buffer (25 mM HEPES pH 7.5, 100 mM NaCl, 0.5 mM EDTA) for 1 h at 37°C to form liposomes. Before mixing with the liposomes, proteins were subjected to centrifugation at 150,000 ***g*** for 15 min at 4°C to remove aggregated portions. Proteins that remained in the supernatant (5 µg) were incubated with the liposomes (25 µg) for 15 min at RT and centrifuged at 150,000 ***g*** for 20 min at 20°C. Proteins that sedimented with liposomes in the pellet and unbound proteins in the supernatant were separated and then subjected to SDS-PAGE followed by Coomassie Brilliant Blue staining.

Acknowledgements

We are grateful to Tomohiko Taguchi for useful discussions and Natsuko Shirai for technical assistance.

Competing interests

The authors declare no competing or financial interests.

Author contributions

Conceptualization: J.H., H.S., M.M., T.I.; Methodology: J.H., I.J., H.Y., E.T., T.I.; Validation: J.H., T.I.; Investigation: J.H., I.J., H.Y., K.T., E.T., T.I.; Resources: J.H., H.S., M.M., T.I.; Writing - original draft: J.H., T.I.; Writing - review & editing: J.H., T.I.; Supervision: T.I.; Project administration: T.I.; Funding acquisition: J.H., T.I.

Funding

This study was supported in part by the Japan Society for the Promotion of Science (JSPS) KAKENHI grant numbers JP24570216 to T.I. and JP24770098 to J.H., the Naito Foundation to J.H., the Sumitomo Foundation to T.I. and the Takeda Science Foundation to T.I.

Supplementary information

Supplementary information available online at
http://jcs.biologists.org/lookup/doi/10.1242/jcs.229179.supplemental

References

Bache, K. G., Brech, A., Mehlum, A. and Stenmark, H. (2003). Hrs regulates multivesicular body formation via ESCRT recruitment to endosomes. *J. Cell Biol.* **162**, 435-442. doi:10.1083/jcb.200302131

Bache, K. G., Slagsvold, T., Cabezas, A., Rosendal, K. R., Raiborg, C. and Stenmark, H. (2004). The growth-regulatory protein HCRP1/hVps37A is a subunit of mammalian ESCRT-I and mediates receptor down-regulation. *Mol. Biol. Cell* **15**, 4337-4346. doi:10.1091/mbc.e04-03-0250

Bonangelino, C. J., Chavez, E. M. and Bonifacino, J. S. (2002). Genomic screen for vacuolar protein sorting genes in Saccharomyces cerevisiae. *Mol. Biol. Cell* **13**, 2486-2501. doi:10.1091/mbc.02-01-0005

Boura, E., Rózycki, B., Herrick, D. Z., Chung, H. S., Vecer, J., Eaton, W. A., Cafiso, D. S., Hummer, G. and Hurley, J. H. (2011). Solution structure of the ESCRT-I complex by small-angle X-ray scattering, EPR, and FRET spectroscopy. *Proc. Natl. Acad. Sci. USA* **108**, 9437-9442. doi:10.1073/pnas.1101763108

Boura, E., Różycki, B., Chung, H. S., Herrick, D. Z., Canagarajah, B., Cafiso, D. S., Eaton, W. A., Hummer, G. and Hurley, J. H. (2012). Solution structure of the ESCRT-I and -II supercomplex: implications for membrane budding and scission. *Structure* **20**, 874-886. doi:10.1016/j.str.2012.03.008

Cai, X., Xu, Y., Cheung, A. K., Tomlinson, R. C., Alcázar-Román, A., Murphy, L., Billich, A., Zhang, B., Feng, Y., Klumpp, M. et al. (2013). PIKfyve, a class III PI kinase, is the target of the small molecular IL-12/IL-23 inhibitor apilimod and a player in Toll-like receptor signaling. *Chem. Biol.* **20**, 912-921. doi:10.1016/j.chembiol.2013.05.010

Campsteijn, C., Vietri, M. and Stenmark, H. (2016). Novel ESCRT functions in cell biology: spiraling out of control? *Curr. Opin. Cell Biol.* **41**, 1-8. doi:10.1016/j.ceb.2016.03.008

Cullen, P. J. (2008). Endosomal sorting and signalling: an emerging role for sorting nexins. *Nat. Rev. Mol. Cell Biol.* **9**, 574-582. doi:10.1038/nrm2427

Dewar, H., Warren, D. T., Gardiner, F. C., Gourlay, C. G., Satish, N., Richardson, M. R., Andrews, P. D. and Ayscough, K. R. (2002). Novel proteins linking the actin cytoskeleton to the endocytic machinery in Saccharomyces cerevisiae. *Mol. Biol. Cell* **13**, 3646-3661. doi:10.1091/mbc.e02-05-0262

Doherty, G. J. and McMahon, H. T. (2009). Mechanisms of endocytosis. *Annu. Rev. Biochem.* **78**, 857-902. doi:10.1146/annurev.biochem.78.081307.110540

Grant, B. D. and Donaldson, J. G. (2009). Pathways and mechanisms of endocytic recycling. *Nat. Rev. Mol. Cell Biol.* **10**, 597-608. doi:10.1038/nrm2755

Hanafusa, H., Ishikawa, K., Kedashiro, S., Saigo, T., Iemura, S.-I., Natsume, T., Komada, M., Shibuya, H., Nara, A. and Matsumoto, K. (2011). Leucine-rich repeat kinase LRRK1 regulates endosomal trafficking of the EGF receptor. *Nat. Commun.* **2**, 158. doi:10.1038/ncomms1161

Hasegawa, J., Tokuda, E., Tenno, T., Tsujita, K., Sawai, H., Hiroaki, H., Takenawa, T. and Itoh, T. (2011). SH3YL1 regulates dorsal ruffle formation by a novel phosphoinositide-binding domain. *J. Cell Biol.* **193**, 901-916. doi:10.1083/jcb.201012161

Hasegawa, J., Strunk, B. S. and Weisman, L. S. (2017). PI5P and PI(3,5)P2: minor, but essential phosphoinositides. *Cell Struct. Funct.* **42**, 49-60. doi:10.1247/csf.17003

Henne, W. M., Buchkovich, N. J. and Emr, S. D. (2011). The ESCRT pathway. *Dev. Cell* **21**, 77-91. doi:10.1016/j.devcel.2011.05.015

Hierro, A., Sun, J., Rusnak, A. S., Kim, J., Prag, G., Emr, S. D. and Hurley, J. H. (2004). Structure of the ESCRT-II endosomal trafficking complex. *Nature* **431**, 221-225. doi:10.1038/nature02914

Hurley, J. H. and Hanson, P. I. (2010). Membrane budding and scission by the ESCRT machinery: it's all in the neck. *Nat. Rev. Mol. Cell Biol.* **11**, 556-566. doi:10.1038/nrm2937

Im, Y. J. and Hurley, J. H. (2008). Integrated structural model and membrane targeting mechanism of the human ESCRT-II complex. *Dev. Cell* **14**, 902-913. doi:10.1016/j.devcel.2008.04.004

Jongsma, M. L. M., Berlin, I., Wijdeven, R. H. M., Janssen, L., Janssen, G. M. C., Garstka, M. A., Janssen, H., Mensink, M., van Veelen, P. A., Spaapen, R. M. et al. (2016). An ER-associated pathway defines endosomal architecture for controlled cargo transport. *Cell* **166**, 152-166. doi:10.1016/j.cell.2016.05.078

Katzmann, D. J., Babst, M. and Emr, S. D. (2001). Ubiquitin-dependent sorting into the multivesicular body pathway requires the function of a conserved endosomal protein sorting complex, ESCRT-I. *Cell* **106**, 145-155. doi:10.1016/S0092-8674(01)00434-2

Korolchuk, V. I., Saiki, S., Lichtenberg, M., Siddiqi, F. H., Roberts, E. A., Imarisio, S., Jahreiss, L., Sarkar, S., Futter, M., Menzies, F. M. et al. (2011). Lysosomal positioning coordinates cellular nutrient responses. *Nat. Cell Biol.* **13**, 453-460. doi:10.1038/ncb2204

Kostelansky, M. S., Sun, J., Lee, S., Kim, J., Ghirlando, R., Hierro, A., Emr, S. D. and Hurley, J. H. (2006). Structural and functional organization of the ESCRT-I trafficking complex. *Cell* **125**, 113-126. doi:10.1016/j.cell.2006.01.049

Lu, Q., Hope, L. W., Brasch, M., Reinhard, C. and Cohen, S. N. (2003). TSG101 interaction with HRS mediates endosomal trafficking and receptor down-regulation. *Proc. Natl. Acad. Sci. USA* **100**, 7626-7631. doi:10.1073/pnas.0932599100

Maxfield, F. R. and McGraw, T. E. (2004). Endocytic recycling. *Nat. Rev. Mol. Cell Biol.* **5**, 121-132. doi:10.1038/nrm1315

Mayor, S. and Pagano, R. E. (2007). Pathways of clathrin-independent endocytosis. *Nat. Rev. Mol. Cell Biol.* **8**, 603-612. doi:10.1038/nrm2216

McCartney, A. J., Zhang, Y. and Weisman, L. S. (2014). Phosphatidylinositol 3,5-bisphosphate: low abundance, high significance. *BioEssays* **36**, 52-64. doi:10.1002/bies.201300012

McMahon, H. T. and Boucrot, E. (2011). Molecular mechanism and physiological functions of clathrin-mediated endocytosis. *Nat. Rev. Mol. Cell Biol.* **12**, 517-533. doi:10.1038/nrm3151

Neefjes, J., Jongsma, M. M. L. and Berlin, I. (2017). Stop or go? endosome positioning in the establishment of compartment architecture, dynamics, and function. *Trends Cell Biol.* **27**, 580-594. doi:10.1016/j.tcb.2017.03.002

Okumura, M., Katsuyama, A. M., Shibata, H. and Maki, M. (2013). VPS37 isoforms differentially modulate the ternary complex formation of ALIX, ALG-2, and ESCRT-I. *Biosci. Biotechnol. Biochem.* **77**, 1715-1721. doi:10.1271/bbb.130280

Olmos, Y. and Carlton, J. G. (2016). The ESCRT machinery: new roles at new holes. *Curr. Opin. Cell Biol.* **38**, 1-11. doi:10.1016/j.ceb.2015.12.001

Pons, V., Luyet, P.-P., Morel, E., Abrami, L., van der Goot, F. G., Parton, R. G. and Gruenberg, J. (2008). Hrs and SNX3 functions in sorting and membrane invagination within multivesicular bodies. *PLoS Biol.* **6**, e214. doi:10.1371/journal.pbio.0060214

Pons, V., Ustunel, C., Rolland, C., Torti, E., Parton, R. G. and Gruenberg, J. (2012). SNX12 role in endosome membrane transport. *PLoS ONE* **7**, e38949. doi:10.1371/journal.pone.0038949

Raiborg, C. and Stenmark, H. (2009). The ESCRT machinery in endosomal sorting of ubiquitylated membrane proteins. *Nature* **458**, 445-452. doi:10.1038/nature07961

Raiborg, C., Bremnes, B., Mehlum, A., Gillooly, D. J., D'Arrigo, A., Stang, E. and Stenmark, H. (2001). FYVE and coiled-coil domains determine the specific localisation of Hrs to early endosomes. *J. Cell Sci.* **114**, 2255-2263.

Raiborg, C., Bache, K. G., Gillooly, D. J., Madshus, I. H., Stang, E. and Stenmark, H. (2002). Hrs sorts ubiquitinated proteins into clathrin-coated microdomains of early endosomes. *Nat. Cell Biol.* **4**, 394-398. doi:10.1038/ncb791

Raiborg, C., Rusten, T. E. and Stenmark, H. (2003). Protein sorting into multivesicular endosomes. *Curr. Opin. Cell Biol.* **15**, 446-455. doi:10.1016/S0955-0674(03)00080-2

Raiborg, C., Wesche, J., Malerød, L. and Stenmark, H. (2006). Flat clathrin coats on endosomes mediate degradative protein sorting by scaffolding Hrs in dynamic microdomains. *J. Cell Sci.* **119**, 2414-2424. doi:10.1242/jcs.02978

Sachse, M., Urbé, S., Oorschot, V., Strous, G. J. and Klumperman, J. (2002). Bilayered clathrin coats on endosomal vacuoles are involved in protein sorting toward lysosomes. *Mol. Biol. Cell* **13**, 1313-1328. doi:10.1091/mbc.01-10-0525

Slagsvold, T., Pattni, K., Malerød, L. and Stenmark, H. (2006). Endosomal and non-endosomal functions of ESCRT proteins. *Trends Cell Biol.* **16**, 317-326. doi:10.1016/j.tcb.2006.04.004

Teo, H., Gill, D. J., Sun, J., Perisic, O., Veprintsev, D. B., Vallis, Y., Emr, S. D. and Williams, R. L. (2006). ESCRT-I core and ESCRT-II GLUE domain structures reveal role for GLUE in linking to ESCRT-I and membranes. *Cell* **125**, 99-111. doi:10.1016/j.cell.2006.01.047

Tonikian, R., Xin, X., Toret, C. P., Gfeller, D., Landgraf, C., Panni, S., Paoluzi, S., Castagnoli, L., Currell, B., Seshagiri, S. et al. (2009). Bayesian modeling of the yeast SH3 domain interactome predicts spatiotemporal dynamics of endocytosis proteins. *PLoS Biol.* **7**, e1000218. doi:10.1371/journal.pbio.1000218

Trajkovic, K., Hsu, C., Chiantia, S., Rajendran, L., Wenzel, D., Wieland, F., Schwille, P., Brügger, B. and Simons, M. (2008). Ceramide triggers budding of exosome vesicles into multivesicular endosomes. *Science* **319**, 1244-1247. doi:10.1126/science.1153124

White, I. J., Bailey, L. M., Aghakhani, M. R., Moss, S. E. and Futter, C. E. (2006). EGF stimulates annexin 1-dependent inward vesiculation in a multivesicular endosome subpopulation. *EMBO J.* **25**, 1-12. doi:10.1038/sj.emboj.7600759

Williams, R. L. and Urbé, S. (2007). The emerging shape of the ESCRT machinery. *Nat. Rev. Mol. Cell Biol.* **8**, 355-368. doi:10.1038/nrm2162

Yu, H., Tardivo, L., Tam, S., Weiner, E., Gebreab, F., Fan, C., Svrzikapa, N., Hirozane-Kishikawa, T., Rietman, E., Yang, X. et al. (2011). Next-generation sequencing to generate interactome datasets. *Nat. Methods* **8**, 478-480. doi:10.1038/nmeth.1597

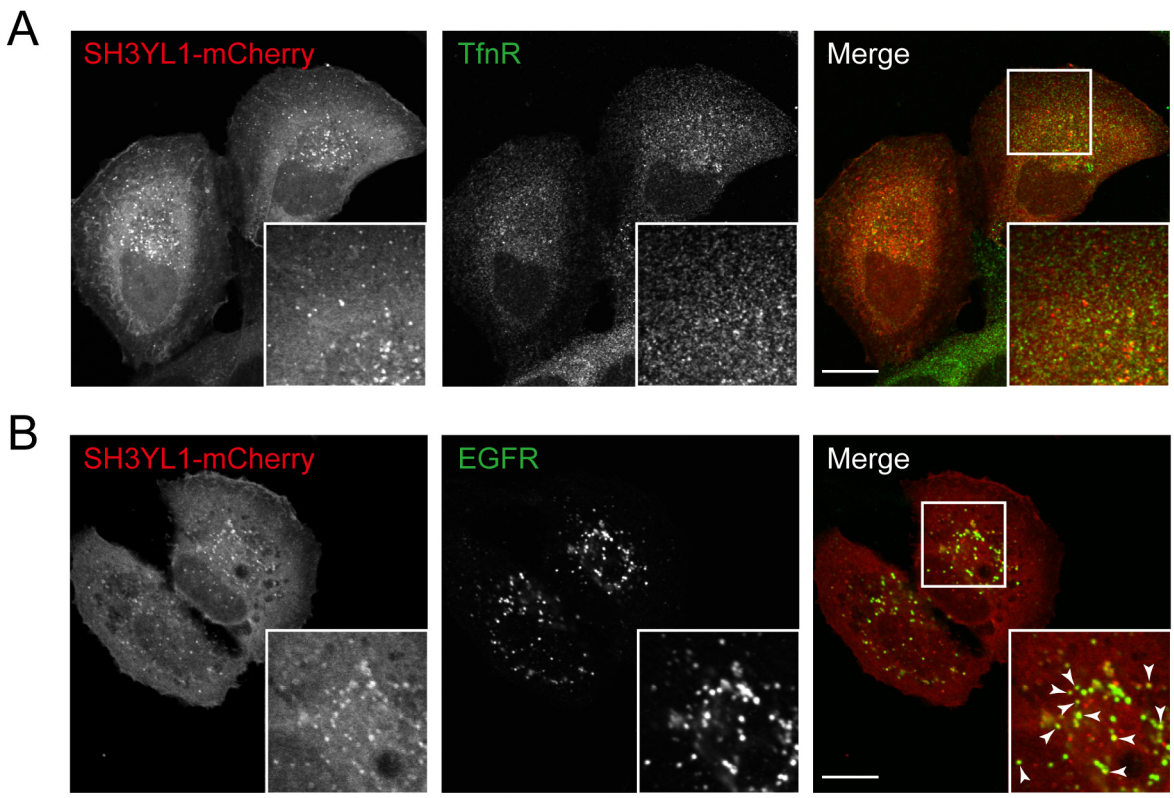

Fig. S1. Localization of SH3YL1 with endosomal markers. (A) HeLa cells stably expressing SH3YL1-mCherry (red) were immunostained with anti-transferrin receptor (TfnR) antibody (green). (B) SH3YL1-mCherry (red) stable HeLa cells were stimulated with 50 ng/ml EGF for 30 min and fixed. The localization of EGFR receptor was assessed by immunostaining with anti-EGFR antibody (green). The boxed region is magnified in inset. Arrowheads indicate colocalizations. Images are representative of three independent experiments. Scale bars, 10 µm.

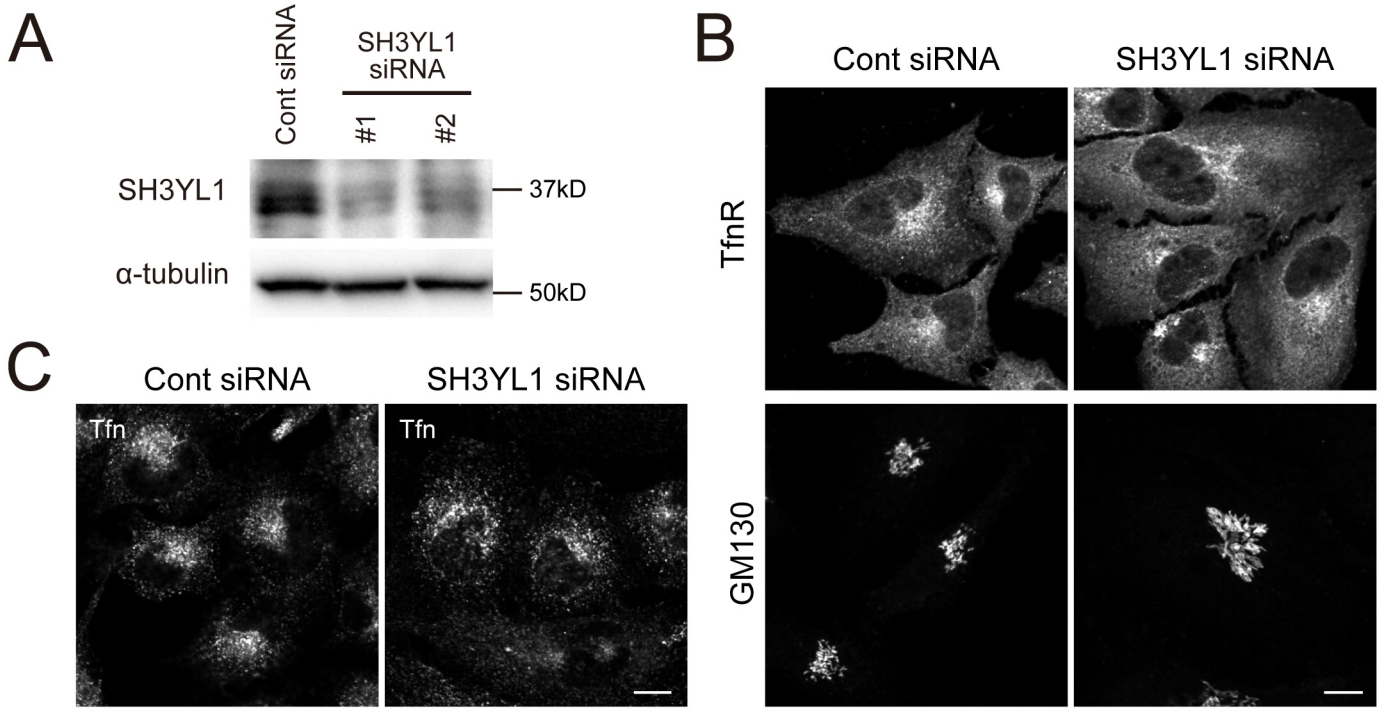

Fig. S2. Depletion of SH3YL1 does not affect transferrin uptake. (A) HeLa cells were treated with control or SH3YL1-specific siRNAs for 72 h, and cell lysates were detected by immunoblotting. (B) SH3YL1 knockdown cells (control or SH3YL1#2) were stained with anti-transferrin receptor (TfnR) or anti-GM130 antibodies. Images are representative of three independent experiments. Scale bars, 10 µm. (C) HeLa cells treated with siRNAs (control or SH3YL1#2) were incubated with 1 µg/ml Alexa Fluor 568-conjugated transferrin (Tfn) for 5 min at 37ºC and then chased in serum-free medium without ligand for 10 min. Images are representative of three independent experiments. Scale bars, 10 µm.

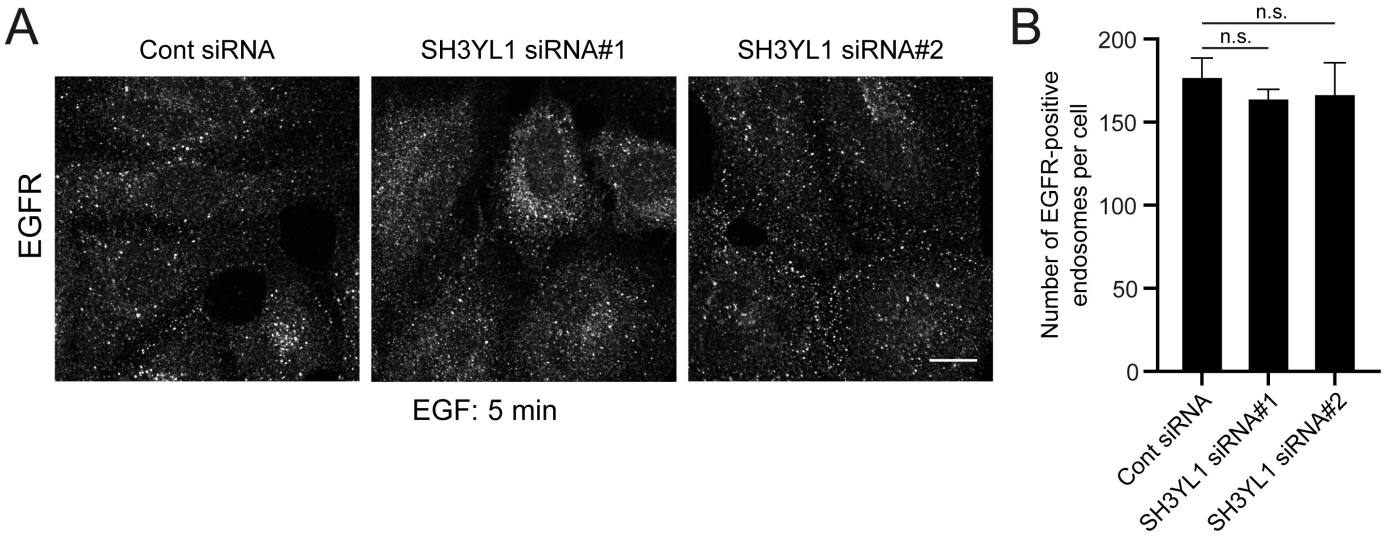

Fig. S3. Depletion of SH3YL1 does not affect EGF uptake. (A) HeLa cells were stimulated with 50 ng/ml EGF for 5 min, fixed, and then immunostained with anti-EGFR antibody. Images are representative of three independent experiments. Scale bars, 10 µm. (B) EGFR-positive endosomes were counted and presented with the mean (±SEM) of three independent experiments with at least 10 cells per experiment. n.s., not significant (Tukey's multiple comparison test).

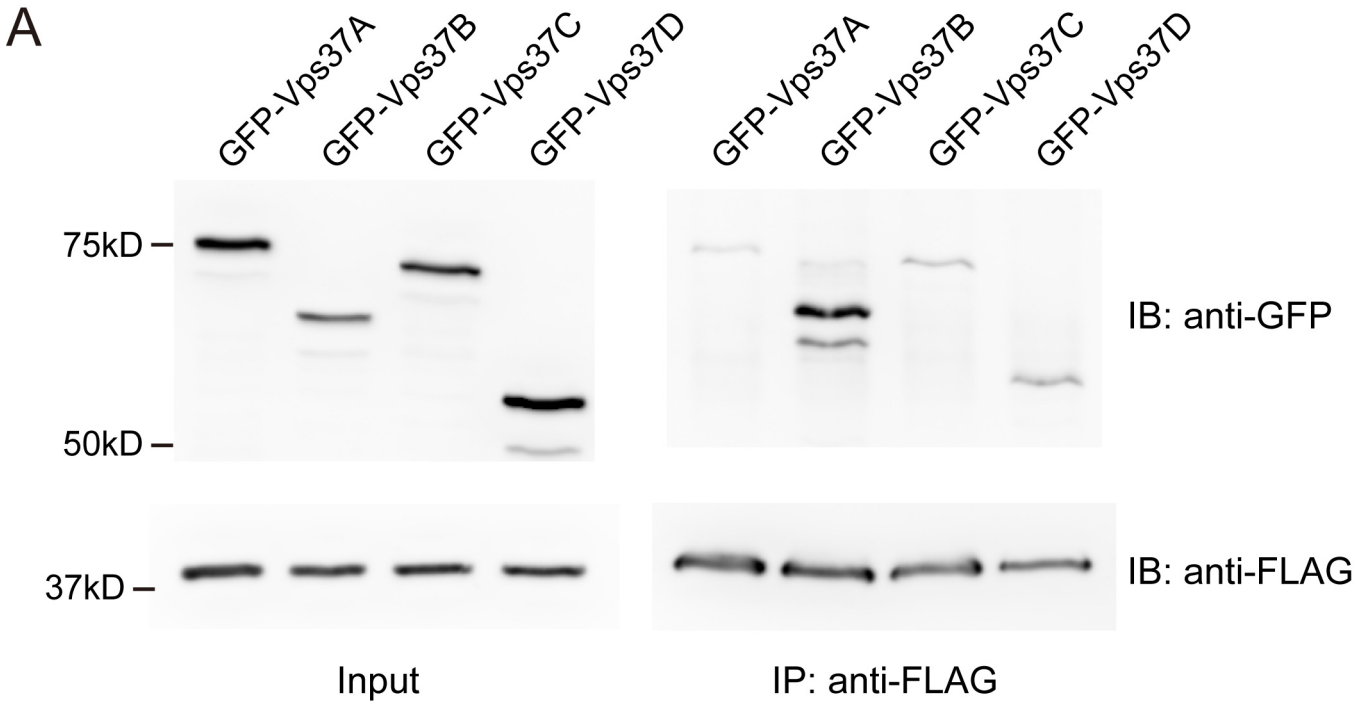

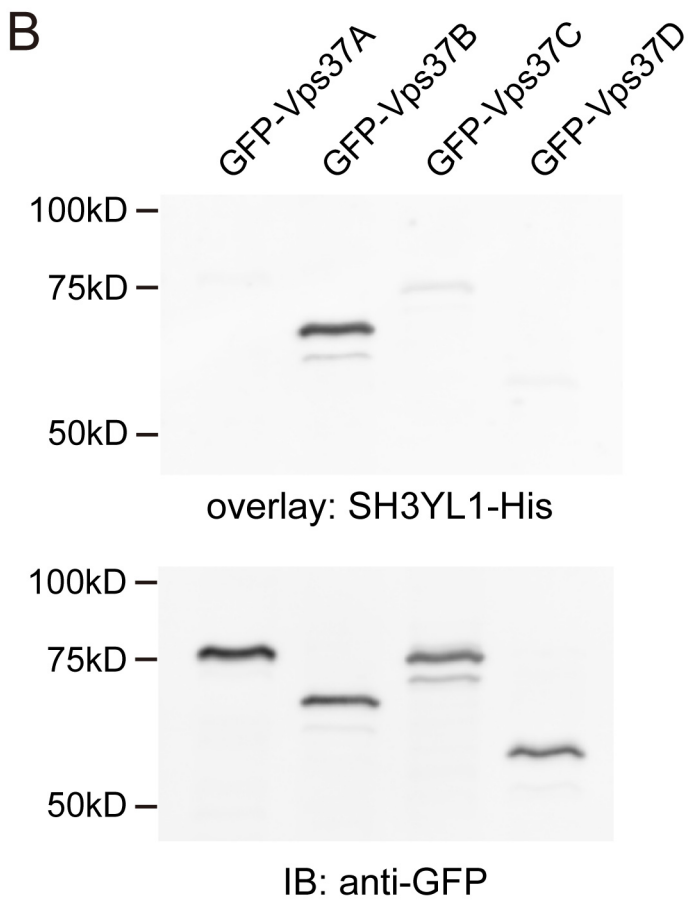

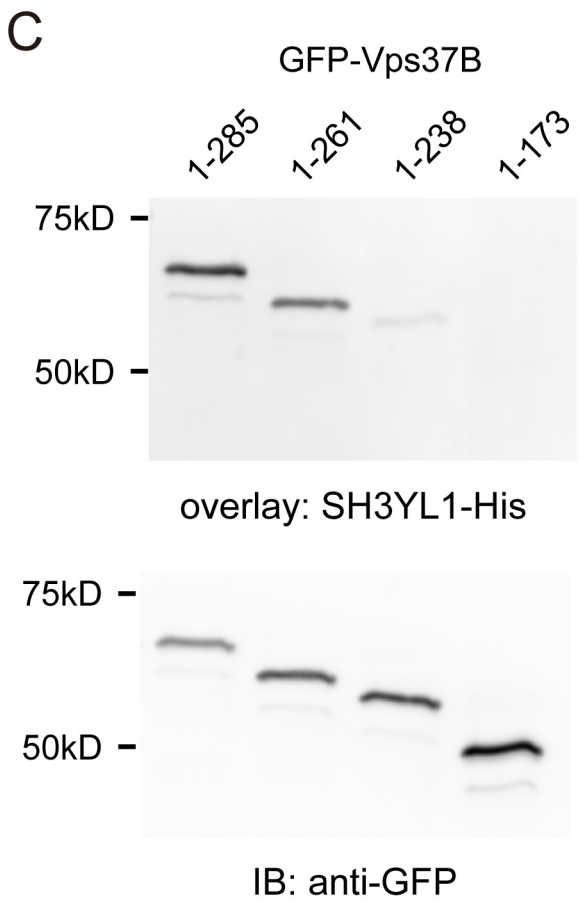

Fig. S4. SH3YL1 binds almost exclusively to Vps37B. (A) Indicated constructs were expressed in 293FT cells together with FLAG-SH3YL1 for 48 h, and cell lysates were prepared. SH3YL1 proteins were immunoprecipitated with anti-FLAG antibody and then analyzed by immunoblotting with anti-GFP antibody. Input; cell lysate. Data are representative of three independent experiments. (B) Indicated constructs of GFP-Vps37 proteins were expressed in 293FT cells and immunoprecipitated with anti-GFP antibody. Immunoprecipitates were transferred onto PVDF membrane after SDS-PAGE and then overlaid by SH3YL1-His recombinant protein (upper). GFP-Vps37 proteins were visualized by western blotting with anti-GFP antibody (lower). Data are representative of three independent experiments. (C) SH3YL1-Vps37B interaction requires “PxLPxR” motifs in Vps37B. Indicated constructs of GFP-Vps37B were subjected to an overlay assay as in (B). Data are representative of three independent experiments.

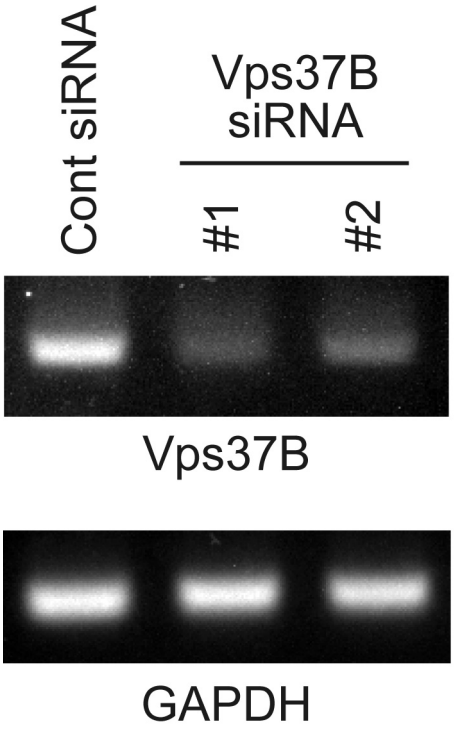

Fig. S5. Knockdown of Vps37B in HeLa cells. HeLa cells were treated with control or Vps37B-specific siRNAs for 72 h. Knockdown levels were assessed by RT-PCR by specific primer sets for human Vps37B (upper) or GAPDH (lower). Data are representative of three independent experiments.

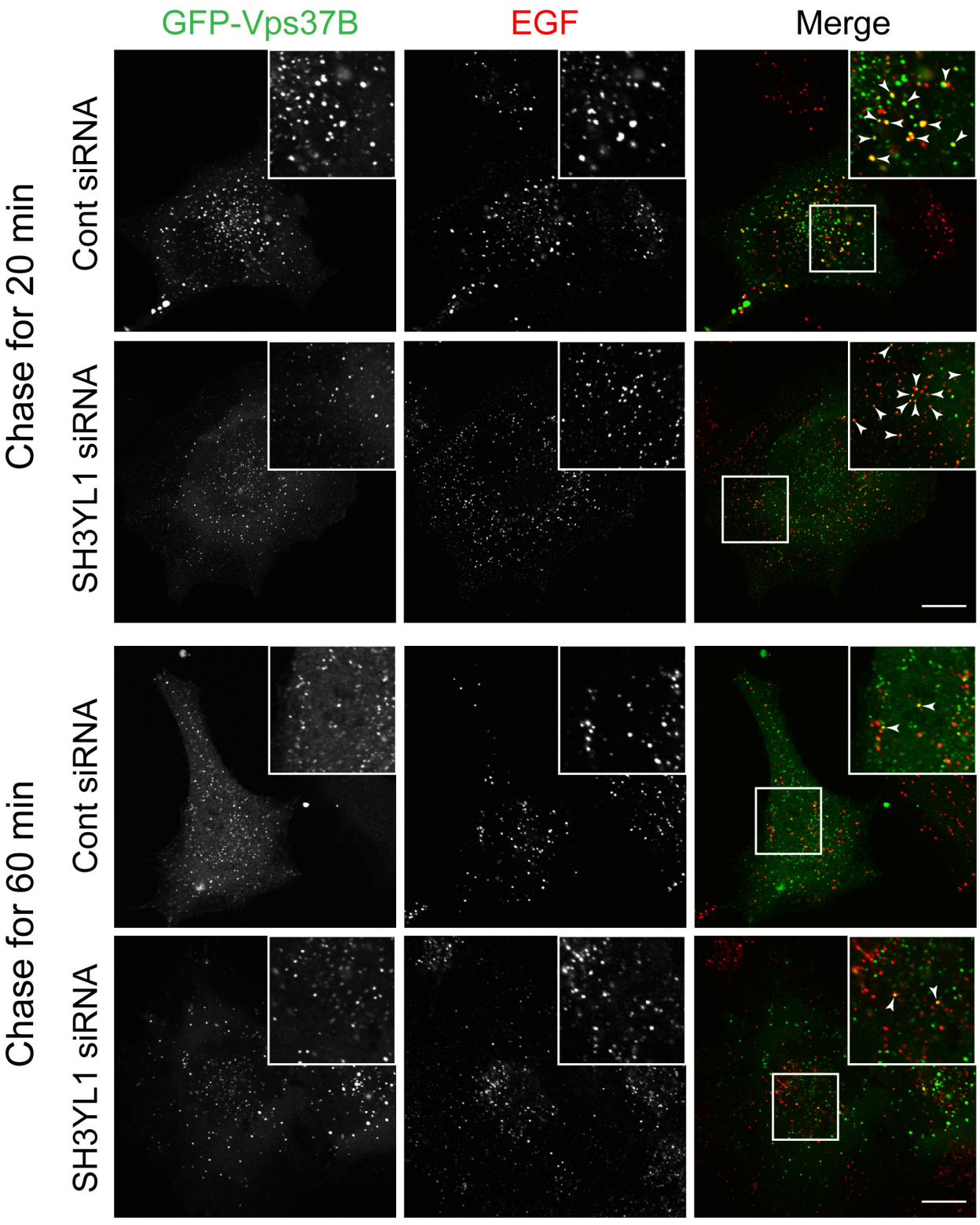
GFP-Vps37B
EGF
Merge
Chase for 20 min
Cont siRNA
SH3YL1 siRNA
Chase for 60 min
Cont siRNA
SH3YL1 siRNA

Fig. S6. Loss of SH3YL1 does not affect EGF trafficking via Vps37B-positive endosomes. (A) HeLa cells co-expressing GFP-Vps37B and mCherry-Tsg101 were treated with siRNAs (control or SH3YL1#2) for 72 h, incubated with 0.1 µg/ml Alexa647-EGF for 5 min at 37ºC and then chased in serum-free medium without EGF for 20 and 60 min. Boxed regions are magnified in insets. Arrowheads indicate colocalization of Alexa647-EGF (red) with GFP-Vps37B (green). Images are representative of three independent experiments. Scale bars, 10 µm. Arrowheads indicate colocalizations with Pearson correlation coefficients of 0.44±0.05 (cont siRNA, 20 min), 0.13±0.08 (cont siRNA, 60 min), 0.29±0.04 (SH3YL1 siRNA#2, 20 min), and 0.13±0.02 (SH3YL1 siRNA#2, 60 min) (mean±SD of 10 cells).

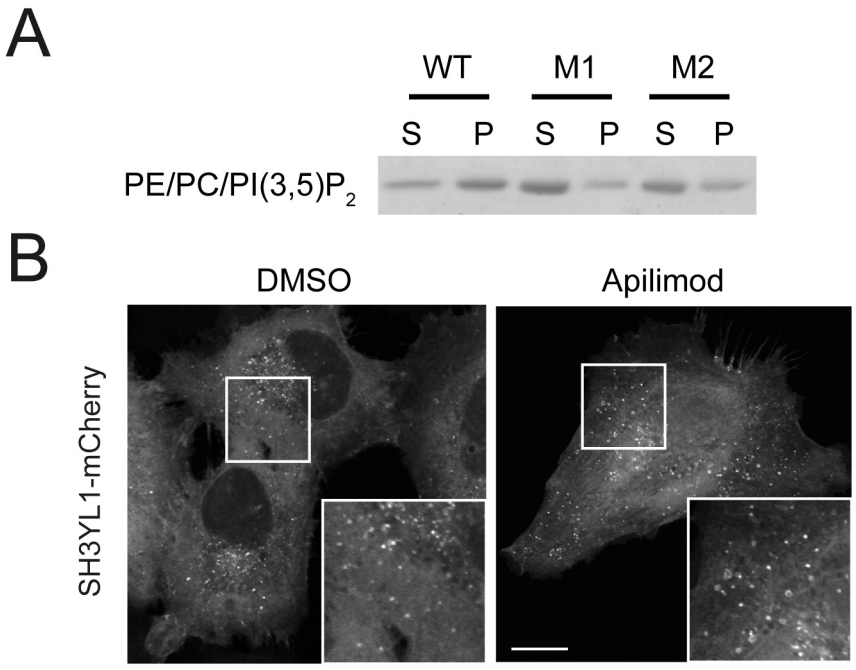

Fig. S7. Vesicular localization of SH3YL1 is not dependent on PI(3,5)P_2. (A) Liposome co-sedimentation assay using PE/PC-based liposomes supplemented with 10% of PI(3,5)P_2 (See Materials and methods in detailed). SH3YL1 recombinant proteins wild-type (WT), amino acid substitutions of $Lys^{14}Lys^{15}$ to $Ala^{14}Ala^{15}$ (M1), and amino acid substitutions of $Lys^{18}Arg^{21}$ to $Ala^{18}Ala^{21}$ (M2) are used in this assay. Data are representative of three independent experiments. **(B)** HeLa cells stably expressing SH3YL1-mCherry were treated by DMSO or 1 μM apilimod (a PIKfyve inhibitor) for 1 h. SH3YL1 is also localized at enlarged endosomes caused by the inhibition of PI(3,5)P_2 synthesis by PIKfyve, indicating its membrane localization is independent of PI(3,5)P_2. Images are representative of three independent experiments.